Digital Comprehensive Summaries of Uppsala Dissertations
from the Faculty of Pharmacy 367

Model-based optimization of cancer immunotherapy combinations

JAVIER SÁNCHEZ FERNÁNDEZ

ACTA UNIVERSITATIS
UPSALIENSIS
2025

ISSN 1651-6192
ISBN 978-91-513-2338-1
urn:nbn:se:uu:diva-544014

UPPSALA
UNIVERSITET

Dissertation presented at Uppsala University to be publicly examined in B21, BMC, Husargatan 3, Uppsala, Friday, 14 February 2025 at 09:15 for the degree of Doctor of Philosophy (Faculty of Pharmacy). The examination will be conducted in English. Faculty examiner: Dinesh De Alwis (Generate Biomedicines).

Abstract
Sánchez Fernández, J. 2025. Model-based optimization of cancer immunotherapy combinations. *Digital Comprehensive Summaries of Uppsala Dissertations from the Faculty of Pharmacy* 367. 70 pp. Uppsala: Acta Universitatis Upsaliensis. ISBN 978-91-513-2338-1.

The use of cancer immunotherapies has transformed the treatment landscape for many cancer types. Unfortunately, not all patients respond to these therapies, and most of those who do eventually relapse. Combining cancer immunotherapies may improve patient outcomes. However, determining which molecules to combine, at which doses, and under which dosing schedules rarely is straightforward.

Preclinical experiments offer the opportunity to test a wide variety of experimental conditions. This data, together with information about disease biology, can be integrated into a mathematical modeling framework, which can be used to simulate different scenarios, allowing researchers to prioritize the most promising drug combinations in the patient populations where the highest probability of success is expected. In a continuous cycle, the model can inform the design of novel biologic drugs with improved pharmacological properties to improve outcomes for a larger percentage of the patient population. This thesis aimed to develop modeling and simulation approaches to guide the development of cancer immunotherapy combinations by contributing to molecule design, preclinical experimental design, and translation of preclinical knowledge into clinical insights.

The translation of the preclinical tumor growth inhibition model suggested that identifying a clinical effect with CD3 T-cell bispecific antibodies in monotherapy may be challenging. However, combination with anti-PD-L1 is expected to more than double progression-free survival, duration of response and response rate, highlighting that combination approaches with these molecules need to be considered as early as possible.

Using preclinical data, a target engagement model for bispecific costimulators was developed that can be used to prospectively predict the clinical range of doses with maximum expected effect. Furthermore, the model allowed differentiating the contribution of drug exposure and target expression to drug pharmacology. Leveraging this model, the impact of binding affinity on drug pharmacology was explored *in silico* for nineteen different oncology indications. This identified a molecule with a 10-fold increase in binding affinity as a promising follow-up molecule that may lead to increased patient benefit, establishing a workflow that can combine preclinical data with clinical target expression to explore *in silico* optimized molecule designs.

Lastly, a novel semimechanistic model was developed to describe clinical pharmacokinetics of biologics under anti-drug antibody formation and associated loss of exposure. The model can be used to accurately establish clinical the dose-exposure-response relationship without excluding patients with loss of drug exposure, as well as to explore the relationship of patient covariates and dosing schedule on drug immunogenicity.

This work highlights how modeling and simulation can leverage preclinical data to answer key clinical questions, such as the expected clinical benefit of a drug combination, the optimal range of doses for molecules with complex exposure-response relationships, and the design of improved molecules. These approaches offer valuable tools for data-driven drug development.

Keywords: pharmacokinetics, pharmacodynamics, oncology, cancer immunotherapy, translational

Javier Sánchez Fernández, Department of Pharmacy, Box 580, Uppsala University, SE-75123 Uppsala, Sweden.

ISSN 1651-6192
ISBN 978-91-513-2338-1
URN urn:nbn:se:uu:diva-544014 (http://urn.kb.se/resolve?urn=urn:nbn:se:uu:diva-544014)

To everyone aiming to develop better medicines

List of Papers

This thesis is based on the following papers, which are referred to in the text by their Roman numerals.

I. Sanchez, J., Nicolini, V., Waldhauer, I., Fahrni, L., Walz, A.C., Simon, S., Fowler, S., Friberg, L.E., Frances, N. (2022) Preclinical In Vivo Data Integrated in a Modeling Network Informs a Refined Clinical Strategy for a CD3 T-Cell Bispecific in Combination with Anti-PD-L1. *AAPS J.*, 1(2):3–4

II. Sanchez, J., Claus, C., Albrecht, R., Gaillard, B.C., Marinho, J., McIntyre, C., Tanos, T., Boehnke, A., Jönsson, S., Friberg, L.E., Frances, N. (2023) A model-based approach leveraging in vitro data to support dose selection from the outset: A framework for bispecific antibodies in immuno-oncology. CPT Pharmacomet Syst Pharmacol. 2023;12(11):1804–18.

III. Sanchez, J., Claus, C., McIntyre, C., Tanos, T., Boehnke, A., Friberg, L.E., Jönsson, S., Frances, N. Combining Mathematical Modeling, in vitro data and clinical target expression to support bispecific antibody binding affinity selection: a case example with FAP-4-1BBL. Front Pharmacol. 2024 Oct 9

IV. Sanchez, J., Pierrillas, P.B., Frey, N., Jönsson, S., Friberg, L.E., Frances, N. A model-based approach 1 to evaluate anti-drug antibody impact on drug exposure with biologics: a case example with the CD3 T-cell bispecific cibisatamab. *In manuscript*

Contents

Abbreviations

AIC	Akaike Information Criteria
CAF	Cancer-associated fibroblast
CEA	Human carcinoembryonic antigen
Cmax	Maximum concentration
CPI	Checkpoint inhibitor
CRC	Colorectal carcinoma
CTLA-4	Cytotoxic T-Lymphocyte Associated Protein 4
DOR	Duration of Response
FAP	Fibroblast Activation Protein
FDA	Food and Drug Administration
FIM	Fisher Information Matrix
GoF	Goodness of Fit
IWRES	Individual Weighted Residuals
LAG3	Lymphocyte-activation gene 3
mAb	Monoclonal antibody
MIDD	Model-informed drug development
MM	Multiple myeloma
MTD	Maximum Tolerated Dose
NHL	Non-Hodgkin's lymphoma
NLME	Nonlinear mixed effects
NSCLC	Non-small cell lung cancer
OCE	Oncology Center of Excellence
ORR	Objective Response Rate
OS	Overall Survival
PBMC	Peripheral blood mononuclear cell
pcVPC	Prediction-corrected Visual Predictive Check
PD-1	Programmed-death-1
PD-L1	Programmed-death-1 ligand
PFS	Progression-free survival
PD	Pharmacodynamics
PK	Pharmacokinetics
RCT	Randomized controlled trial

RP2D	Recommended Phase 2 Dose
s.c.	sub-cutaneous
SAEM	Stochastic Approximation-Expectation Maximization
SLD	Sum of Longest Diameters
TCB	T-cell bispecific
TCR	T-cell receptor
TIGIT	T cell immunoreceptor with immunoglobulin and ITIM domain
TIM-3	T-cell immunoglobulin and mucin-domain containing-3
TYRP1	Tyrosinase-related protein 1

Introduction

Cancer immunotherapies aim to redirect the patient's own immune system against tumor cells. To date, different molecules directed against a variety of targets have been approved by regulatory authorities, offering transformational treatments to patients afflicted by more than thirty different cancer types (1). Nevertheless, up to 85% of the patients do not respond to these cancer immunotherapies (2), which motivates the search for novel molecules with different mechanisms of action.

It has been proposed that the use of combination therapies with cancer immunotherapies can further improve patient outcomes (3). To inform which molecules to combine, at which doses, and in which patient population, data from different sources can be integrated into a mathematical modeling framework (4). Such models can then be used to simulate different scenarios, allowing researchers to prioritize the most promising drug combinations in the patient populations where the highest probability of success is expected.

In a continuous cycle, the developed models can also inform the design of novel biologics with improved pharmacological properties that can potentially improve outcomes for a larger percentage of the patient population (5).

Cancer Immunotherapy

Overview

Cancer immunotherapy can be defined as a series of therapies that make use of components of the immune system to fight against tumor cells (6). Broadly, two classes of cancer immunotherapies are recognized: off-the-shelf therapies and patient-specific engineered products (7). The former consists of treatments (usually antibody-based) which are manufactured at a large scale, independent of the patient they aim to treat. The latter, conversely, comprises treatments (usually based on genetically modified T cells) which are manufactured using cells from each specific patient (8). Despite transformative efficacy when treating hematological malignancies (9,10), patient-specific engineered products have a long manufacturing time, which frequently precludes their use in patients with aggressive disease and short life-expectancy (11). Because these products need to be manufactured on a personalized basis for each patient, scalability of manufacturing is a challenge (12), which further

complicates access to these therapies. Furthermore, the efficacy of patient-specific engineered products in solid tumors has underwhelmed when compared to hematological malignancies (13).

On the other hand, off-the-shelf cancer immunotherapies simplify many of these challenges: they can be easily manufactured at scale, are immediately ready for administration following disease diagnosis or relapse, and have shown comparable efficacy in hematological malignancies (14). Nevertheless, similar to what has been observed with patient-specific engineered products, outcomes in patients with solid tumors have not been improved as much as for patients with hematological malignancies (15). Different classes of off-the-shelf cancer immunotherapies have been approved by regulatory authorities in the last decade, each with unique characteristics and aimed at specific components of the immune system. These classes are described in more detail below and comprise checkpoint inhibitors (CPIs) and T-cell bispecific antibodies (TCBs).

Tumor-immune system interplay

It is increasingly recognized that the immune system status plays a key role in tumorigenesis, tumor prognosis and response to treatment (16). In fact, tumors can be classified in inflamed, excluded or immune desert tumors according to the presence or absence of immune cells in the tumor microenvironment, as well as based on the status of such immune cells (17). For example, immune-inflamed tumors are characterized by high levels of immune cell infiltration, and frequently respond better to cancer immunotherapy (18). Melanoma and non-small cell lung cancer (NSCLC) are usually considered as an example of immune-inflamed tumors. Immune excluded tumors, on the other hand, are characterized by the presence of immune cells confined to the periphery of the tumor. This immune phenotype is characteristic of breast or ovarian cancer (19). Finally, immune desert tumors show no presence of immune cells at all, neither in the periphery nor in the tumor mass. Examples of immune desert tumors are most cases of colorectal carcinoma (CRC) or glioblastoma. Immune desert tumors present the lowest response rates to cancer immunotherapy to date, despite comprising some of the most frequently diagnosed cancer types.

In addition to tumor and immune cells, other cell types play an important role in tumor prognosis. Specifically, cancer-associated fibroblasts (CAFs) are increasingly recognized as a key driver of the aggressiveness of some tumor types (20). On the other hand, the unique features of CAFs (as compared to normal fibroblasts in other tissues) present the opportunity of using them as targets for novel treatments (21,22).

Checkpoint inhibitors

In healthy individuals, the immune system is capable of rapid and selective activation upon detection of pathogens or tumoral markers. Once these pathogens or tumoral cells have been eliminated, the immune system returns to its active surveillance state, and the immune response is winded down (23). Checkpoint proteins are molecules routinely expressed by the immune system, whose function is, precisely, to decrease immune response after the threat that triggered immune activation has been counteracted (24). However, in many tumors, different cell types in the tumor microenvironment can express or induce the expression of these checkpoint proteins, effectively preventing the immune response against the tumor (25).

Although several checkpoint proteins exist, the most extensively researched comprise the Programmed Death-1 (PD-1) and Programmed-Death-1 Ligand (PD-L1) axis (26). The blockade of PD-1 (usually expressed on immune cells) and PD-L1 (usually expressed on tumor cells) is capable of restoring the activation status of exhausted T cells within the tumor microenvironment (27). This has led to the development of several CPIs targeting PD-1 and PD-L1. To date, more than eight different PD(L)-1 CPIs have been approved by the Food and Drug Administration (FDA) of the United States in more than 30 different oncology indications (1).

In addition, CPIs against the Cytotoxic T-lymphocyte-associated Protein 4 (CTLA-4) and Lymphocyte-activation Gene 3 (LAG3) have also been approved by regulatory authorities (28–30), although not across as many indications as PD(L)-1 inhibitors. Several pivotal clinical trials exploring PD-(L)1 CPIs in combination with T-cell immunoglobulin and mucin-domain containing-3 (TIM-3) and T cell immunoreceptor with immunoglobulin and ITIM domain (TIGIT) blockade are ongoing (31,32).

Despite transformational results in tumor types with high levels of T-cell infiltration and/or high levels of PD-L1 expression, PD(L)-1 CPIs generally do not elicit responses in immune excluded tumor types (33,34). Even among immune inflamed tumor types, the highest response rates to single-agent CPI are found in the PD-L1-high subgroup of NSCLC, where up to 45% of patients responded to the PD-1 inhibitor pembrolizumab (35).

The combination of CPIs directed against different targets (*e.g.* PD-1 and CTLA-4, PD-1 and LAG3, or PD-L1 and TIGIT inhibitors) has shown higher response rates than single-agent PD(L)-1 blockade across different trials (36–38). However, its use currently remains confined to immune inflamed tumors.

CD3 T-cell bispecific antibodies

T-cell bispecific antibodies (TCBs) are capable of binding simultaneously to a receptor expressed on the T-cell surface (frequently CD3) and to a tumor-specific antigen on the surface of tumor cells (39). In doing so, TCBs can form

a molecular entity termed trimeric complex (bispecific antibody bound simultaneously to both targets). This trimeric complex formation can promote T-cell activation and elicit tumor cell killing via cytotoxicity (40,41). While CPIs are capable of restoring exhausted and inactive T cells (27), their ability to promote *de novo* T-cell infiltration into tumors is controversial (42). Conversely, TCBs have been shown to drive immune cell infiltration in immune excluded tumors, both preclinically (41,43) and in the clinic (44). As such, they represent a promising strategy to treat tumor types traditionally considered unresponsive to CPIs.

To date, several CD3 TCBs have been approved for the treatment of hematological malignancies, such as non-Hodgkin lymphoma (NHL) (45–47) and multiple myeloma (MM) (48–50). In solid tumors, however, TCBs have been associated with transient efficacy, frequently followed shortly after by tumor regrowth (44,51). It has been proposed that such short-lasting effects could be associated with T-cell exhaustion phenomena (52,53), loss of tumor target expression (54) or development of anti-drug antibodies (ADAs) against the TCB (55,56).

To improve on the results obtained so far with single-agent TCBs in solid tumors, combination with other cancer immunotherapies (such as CPIs) have been tested both preclinically (57,58) and in clinical trials (44). Moreover, additional strategies to further activate T cells by stimulating other T-cell receptors are also being tested (22,59).

Tumor-targeted costimulators

Initial T-cell activation usually takes place via the T-cell receptor (TCR), of which the CD3 subunit targeted by CD3 TCBs constitutes an essential component (60). This first activation is also known as *Signal 1*. When T cells are subjected to *Signal 1* activation, other receptors are expressed or overexpressed. Some of these receptors are known as costimulatory receptors, and can provide additional T-cell activation, prevent T-cell exhaustion and enhance tumor cell killing (61–63). As such, they represent a logical target for the development of cancer immunotherapies.

The 4-1BB (also known as CD137) (62) and CD28 receptors (63) are classic examples of costimulatory proteins for T cells. Although attempts have been made at stimulating both 4-1BB and CD28 to promote T-cell activation, the use of agonistic monoclonal antibodies (mAbs) resulted in systemic T-cell activation and severe hepato- and nephrotoxicity (64,65).

To overcome these safety liabilities, bispecific antibodies providing T-cell costimulation only while simultaneously bound to a tumor-specific target have been developed (22,66,67). *Figure 1* represents schematically the biological rationale to combine TCBs with tumor-targeted bispecific costimulators. Several of these tumor-targeted costimulators are in clinical trials, both in combination with CPIs and CD3 TCBs.

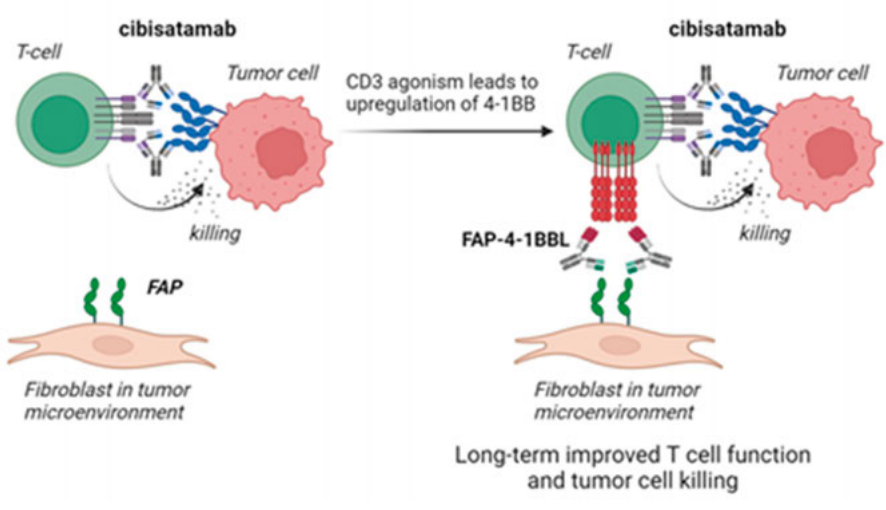

Figure 1. Schematic representation of the interplay between *Signal 1* (provided by the CD3 TCB cibisatamab) and *Signal 2* (provided by the tumor-targeted costimulator FAP-4-1BBL) to achieve improved T-cell activation in a tumor-specific manner.

Of note, the tumor-specific target used for the tumor-specific costimulator does not necessarily need to be expressed by tumor cells, provided that it is expressed on other cell types (*e.g.* CAFs) present in the tumor microenvironment.

Treatment response evaluation in solid tumors

When cancer patients undergo treatment (both in clinical practice or inside a clinical trial) it is important to evaluate how the course of the disease is evolving. In the particular context of clinical trials, however, change in tumor burden (comprising both tumor shrinkage as well as tumor growth) are frequently used as endpoints and also guide physicians' decisions about whether therapy should be discontinued.

In the case of solid tumors, well-defined criteria have been proposed to objectively delineate what constitutes a worsening in disease, a decrease in tumor burden which can be attributed to the therapy or the baseline characteristics that patients must fulfill to be evaluable as per these criteria. Originally published in the year 2000, these guidelines, termed Response Evaluation Criteria in Solid Tumors (RECIST) has been slightly updated (68).

The RECIST criteria is of particular interest when dealing with mathematical models and simulations of tumor growth and shrinkage, as it defines quantitatively what constitutes both a response and a disease progression event (which, perhaps equivocally, involves a worsening of the disease). To do so, the RECIST criteria focuses on two types of lesions or metastasis that may be present in patients at the time of inclusion in the clinical trial: target and non-target lesions. The guidelines also specify the criteria that the specific tumor lesions must fulfill to qualify as target. In brief, target lesions are characterized by being measurable at baseline, and their size can therefore be followed over time. Although both play an important role in defining both tumor response and disease progression, only target lesions are evaluated quantitatively, being therefore of greater importance when aiming to fit mathematical models to tumor measurements. In the explanations that follow, only the tumor shrinkage and growth criteria that need to be met for target lesions to trigger response and disease progression are discussed.

As per RECIST, a response is defined as a shrinkage of at least 30% from baseline in the sum of longest diameters (SLD) of up to five tumor lesions designated by the investigator as target lesions. The total disappearance of all evidence of cancer disease is termed "complete response", whereas a tumor shrinkage meeting the criteria of response but showing evidence of disease (either in target or non-target lesions) is termed partial response. In many clinical trials (particularly those with response rate as primary endpoint), a response (partial or complete) needs to be confirmed in two different tumor scans at least four weeks apart if the patient is to be considered a responder.

On the other hand, disease progression (when focusing only on target lesions) is defined as at least a 20% increase in the SLD from the nadir (minimum SLD recorded, whether at baseline or on treatment). Additionally, the absolute SLD increase (*i.e.* the difference between the nadir SLD and the SLD that triggers the progression event) must be at least 5 mm. It is important to note that other factors (like appearance of new tumor lesions) can also trigger a progression event regardless of changes in SLD.

Lastly, changes in SLD that qualify neither as partial response nor as disease progression are referred to as stable disease. When evaluating the best response to treatment for a given patient, if that best response is stable disease, a minimum duration of stable disease (frequently 12 weeks) also needs to be met.

By using these guidelines, several endpoints can be calculated, such as objective response rate (ORR, percentage of patients with partial or complete response as best response to treatment), progression-free survival (PFS, frequently summarized as median [if reached at the data cutoff]), and duration of response (DOR, time between the first tumor assessment deemed to be either a partial or complete response, and disease progression).

Preclinical models for drug development in oncology

In vitro systems

One of the simplest methods to inform early drug development are *in vitro* systems, where cells are cultured in culture plates in a laboratory. The ease of use of *in vitro* experiments allows testing a wide variety of conditions in a homogeneous, low-variability and well-controlled system. Of special use in cancer immunotherapy are experimental set-ups where different cell types are cultured together. Such systems can include not only tumor cells, but also immune cells and even components of the tumor microenvironment, such as fibroblasts (22,54).

Thus, these systems allow evaluating different metrics, such as tumor cell killing, cytokine release or T-cell activation markers. Furthermore, different concentrations of the drug of interest can be tested to establish the concentration-response relationship of different endpoints of interest, such as tumor cell killing, cytokine release or T-cell activation. A unique aspect of research with CD3 TCBs and tumor-targeted costimulators is that they require simultaneous binding to two different targets to elicit their activity. As such, *in vitro* systems present the unique opportunity of simultaneously evaluating not only the effect of different drug concentrations, but also the effect of different numbers of receptors per cell and different proportions of cell types.

For *in vitro* cancer immunotherapy research, the source of immune cells is frequently human peripheral blood mononuclear cells (PBMCs) isolated from the blood of donor samples. These samples can also reflect, to some extent, the interindividual variability that may be expected in humans.

In vivo models

Although *in vitro* systems have evolved into more complex set-ups that can better recapitulate biological aspects of the human patient, unique aspects of a drug's pharmacology can only be evaluated *in vivo*. The pharmacokinetics (PK, what the body does to the drug) of an antibody, for example, can be accurately anticipated in the clinic based on the PK profile of the same drug in preclinical species (69). In the specific case of cancer immunotherapy, the changes in the immune system over time (*e.g.* time from treatment to T-cell activation, dynamics of T-cell expansion and exhaustion while on treatment) are of the utmost importance to design rational clinical trials, select appropriate doses and dosing schedules and maximize the chance of success by selecting the best combination partner for each molecule. Although current *in vitro* systems allow time-course experiments to some extent, the maximum duration for such experiments is typically of up to five days (70).

Conversely, experiments in mouse xenograft models can be conducted to simultaneously evaluate the PK and dose-response relationship of anticancer

drugs (71). Mice xenografts consist of immunosuppressed mice that have been subcutaneously injected with tumor cells, which are able to form a functional tumor. Once the implanted tumor reaches a certain volume, drugs can be tested and their effect on tumor volume can be evaluated over multiple days. Although these models have been used for decades in oncology drug development, their use for cancer immunotherapy research poises unique challenges. For example, it is frequent that antibodies designed to bind to a human receptor are not cross-reactive in the mouse (*i.e.* the antibody does not bind to the mouse receptor) or engage the receptor with a different binding affinity as compared to the human. Moreover, the immune system of the mouse may behave differently than that of the human and is therefore usually suppressed to avoid rejection of the tumor implant.

To circumvent these challenges, humanized mouse models have been developed and refined in recent years (72). These models offer the possibility of testing cancer immunotherapies in mice whose immune system consists (at least partially) of human cells. Although model-specific differences exist, humanized mice models are usually generated by treating young mice with busulfan and other chemotherapeutic agents to deplete the bone marrow. Later, adoptive cell transfer with human PBMCs is performed, after which the mouse is engrafted with human immune cells (73).

Humanized mouse models have been successfully used to evaluate different formats of cancer immunotherapy, both as single-agent and in combination with other drugs (57).

Early clinical development in oncology

The maximum-tolerated-dose paradigm

In drug development, the primary objective of Phase I, first-in-human, trials is always to establish the safety of the investigational drug. As such, Phase I trials are designed to progressively increase the tested dose while carefully monitoring the trial participants for safety signals. Phase I trials in oncology have certain particularities compared to other therapeutic areas, as they are usually conducted in patients rather than healthy volunteers (74). In consequence, first-in-human dose selection poses unique challenges, as it needs to balance safety while ensuring that patients are not exposed to unnecessarily low doses that fail to elicit any biological effect. Furthermore, dose escalation in the trial is not always straightforward, as safety signals may emerge which can be both attributable to the drug and the course of the disease.

In oncology, Phase I trials have also traditionally aimed to establish the Maximum Tolerated Dose (MTD), defined as “the highest dose of a drug or a treatment that does not cause unacceptable side effects”. Because oncology drug development started with cytotoxic drugs, for which drug activity

typically increases with increasing dose or exposure, the MTD was effectively used in many cases to select the efficacious dose. This paradigm may not apply to novel therapeutic classes (such as targeted therapies or cancer immunotherapy), which can display different exposure-response profiles (75), and regulators are increasingly recognizing that more rational approaches to select efficacious doses are needed (76).

To this regard, understanding the relationship between drug exposure, drug safety, and drug efficacy as early as possible has become crucial to successfully developing novel oncology therapeutics.

Immunogenicity with biologic drugs

Most of the approved and investigational off-the-shelf cancer immunotherapies are protein-like biologics based on mAbs. Given that many antibody-based products undergo bio-engineering to refine pharmacological properties, amino acid sequences differing from typical human immunoglobulins are common (77). As a result, the administration of therapeutic antibodies can induce an immune response in the treated patient, which frequently leads to the development of ADAs. The development of ADAs has been associated with increased clearance of the therapeutic protein from the systemic circulation (55,56), decreased efficacy (78,79) and increased safety concerns (78,80). The evaluation of immunogenicity and the characterization of its impact on drug pharmacology is therefore an important focus of early clinical trials with biologics in oncology.

Mathematical models for drug development

Nonlinear mixed effects models

It is common that during drug development, PK and pharmacodynamics (PD) data are gathered from several subjects (animals during preclinical development and healthy volunteers or patients during clinical trials). Nonlinear mixed effects (NLME) models are a mathematical framework to simultaneously describe the typical and individual PK or PD of a studied population. To do so, an average or typical value of a model parameter is estimated, as well as its variability in the population, without the need to explicitly estimate individual parameters for each subject. To do so, NLME models account for both fixed effects (common to the population) and random effects (individual variability).

The use of NLME models in the context of analyzing pharmacology data is often termed population approach. Currently, these models are used not only to describe data, but also to optimize dosing regimens and support decision-making across all stages of drug development.

Tumor growth inhibition models

Tumor growth inhibition models are a particular type of mathematical model aiming to describe the tumor growth, shrinkage and/or emergence of resistance to treatment. A wide variety of TGI models have been developed for different purposes, leveraging data both from clinical trials, as well as from preclinical species (81).

Unperturbed tumor growth can range from simple linear or exponential models to more complex models describing saturation of tumor growth when the tumor burden approaches a maximum capacity (82). With regards to the effect of drugs on tumor kinetics, these are frequently assumed to either decrease the growth rate (83) or increase the death rate of the tumor (84). Different mechanisms have been proposed to explain the development of resistance to treatment, including preexisting cell populations resistant to treatment (84) or transitions from sensitive to resistant phenotypes over time (85). *Figure 2* schematically represents an example of a TGI model describing unperturbed tumor growth, tumor shrinkage as a result of drug administration, and tumor regrowth due to resistance emergence.

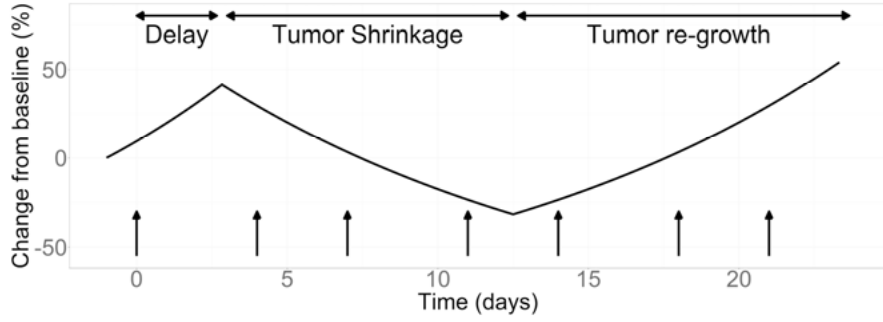

Phase					
Effect	Delay	Transition	Tumor Shrinkage	Transition	Tumor re-growth
Growth	$k_{GROW_{sensitive}}$	*Time to treatment effect*	$k_{GROW_{sensitive}}$	*Time to tumor regrowth*	$k_{GROW_{resistant}}$
Killing	–		$k_{DEATH\ Max}, EC_{50}$		–

Figure 2. Schematic representation of the different tumor growth inhibition phases that can be described using a mathematical model.

Target engagement models

To exert their pharmacological effect, all drugs need to engage (*i.e.* bind) their target. Accounting for drug-target binding can serve as an intermediate step towards elucidating the exposure-response relationship, and can also aid in the translation between preclinical and clinical stages of drug development (86).

In the case of TCBs and tumor-targeted costimulators, target engagement becomes of even more importance: two targets need to be simultaneously engaged for the drug to exert its pharmacological effect. As such, modeling target engagement with bispecific antibodies has become a standard technique to establish the PK/PD properties of these therapeutics.

Several models for target engagement with bispecific antibodies have been described so far, ranging from sequential binding assuming a well-stirred system (87) to more complex binding models that account for antibody immobilization after the first binding step (88).

These models have already been used to propose both safe starting doses in the clinic (86), as well as to suggest patient populations for which increased treatment benefit is expected (70).

Relevant molecules for the performed work

TYRP1-TCB

The Tyrosinase-related protein 1 (TYRP1) is a membrane protein overexpressed by certain melanoma tumors (89,90). As such, it represents a promising target when treating this malignancy. TYRP1-TCB (RO7293583) is a CD3 TCB capable of simultaneously binding to TYRP1 on the melanoma cells, and CD3 on the T cells. In doing so, it promotes T cell activation and tumor cell killing (58). The clinical strategy to develop TYRP1-TCB was explored in Paper I.

FAP-4-1BBL

FAP-4-1BBL (RO7122290) is a bispecific capable of binding the Fibroblast Activation Protein (FAP), overexpressed in CAFs and tumor-draining lymph nodes (89,90). FAP-4-1BBL is also capable of binding the 4-1BB costimulatory receptor, expressed on activated T cells. When simultaneously engaging both FAP on fibroblasts and 4-1BB on T cells, FAP-4-1BBL forms an entity termed trimeric complex, which is capable of providing tumor-specific 4-1BB costimulation (as FAP expression is restricted to tumor and draining lymph nodes).

FAP-4-1BBL has been studied in the clinic both as a single agent, in combination with the PD-L1 inhibitor atezolizumab, and in combination with the TCB cibisatamab. In Paper II, a modeling and simulation workflow leveraging *in vitro* data to inform clinical dose selection and explore the biomarker-drug activity relationship is proposed using the case-example of FAP-4-1BBL in combination with cibisatamab. In Paper III, the quantitative insights about FAP-4-1BBL pharmacology gained in Paper II are used to propose alternative molecular designs for follow-up FAP-targeted 4-1BB

costimulators with enhanced pharmacological properties using solely *in silico* modeling and simulation.

Cibisatamab

Cibisatamab is a CD3 TCB antibody directed against the human carcinoembryonic antigen (CEA). Similar to TYRP1-TCB, it can trigger T-cell activation and tumor cell killing upon binding of both CEA and CD3. Cibisatamab has been studied in patients with advanced, CEA-positive solid tumors both in monotherapy and in combination with the anti-PD-L1 checkpoint inhibitor atezolizumab and the bispecific costimulator FAP-4-1BBL.

In Paper II, the relationship between cibisatamab concentration and 4-1BB expression on T cells over time was quantified using a semimechanistic model build using *in vitro* data. In Paper IV, a population PK model is developed using clinical PK samples from two cibisatamab studies.

Aims

The aim of this thesis was to develop modeling and simulation approaches to guide the development of cancer immunotherapy combinations by contributing to molecule design, preclinical experimental design, and translation of preclinical knowledge into clinical insights. Moreover, it sought to develop methodology to guide the clinical development of cancer immunotherapy combinations by efficiently optimizing the drug dose and dosing schedule. Such objective is in line with the Oncology Center of Excellence (OCE) *Project Optimus* at FDA, which aims to change the paradigm of how doses are currently selected in oncology drug development. In addition, it aimed to provide recommendations on how preclinical modeling and simulation can support the clinical development of cancer immunotherapy combinations, and how it can inform the design of follow-up molecules with enhanced pharmacological properties. The specific aims of the projects were as follows:

- To develop a tumor growth inhibition model using *in vivo* mouse xenograft data to guide early clinical development of TCBs in combination with CPIs in solid tumor indications (Paper I).

- To develop a target engagement model linking target expression, bispecific costimulator exposure and increase in tumor cell killing to support clinical dose selection and biomarker strategy (Paper II).

- To explore *in silico* the impact of binding affinity in expected pharmacological effect to inform the design of novel tumor-targeted costimulators taking into account information on clinical target expression (Paper III).

- To develop a population model describing the PK, the formation of ADAs and their impact on drug exposure using data from patients with advanced solid tumors treated with cibisatamab (Paper IV).

Methods

Data

Data from both preclinical and clinical settings were used to develop the models. The preclinical data consisted of both *in vivo* and *in vitro* measurements. The clinical data were available from two Phase I/Phase Ib clinical studies. Additionally, in Paper III, simulated data were generated.

Preclinical *in vivo* data (Paper I)

Sixty-six humanized mice (*i.e.* with immune systems partly consisting of human cells) received a single sub-cutaneous (s.c.) injection with two million TYRP1-expressing tumor cells derived from melanoma patients. Twenty-four days after s.c. implantation of the tumor cells (when the tumors reached a volume of approximately 120 mm^3), the mice were randomized in six different groups consisting of eleven individuals each. Randomization was stratified by tumor volume and humanization degree (percentage of human immune cells).

The control group received histidine buffer as vehicle. Four different doses of TYRP1-TCB as single agent (0.02, 0.1, 0.5 and 2.5 mg/kg) and a single dose (2.5 mg/kg) of TYRP1-TCB combined with anti-PD-L1 at a dose of 10 mg/kg were tested. TYRP1-TCB was administered twice per week for a total of 7 administrations, while anti-PD-L1 was administered weekly.

Daily controls for detection of adverse effects were performed. Mice were weighed every week, and tumor growth was measured by digital caliper three times a week. Termination criteria for animals were visible sickness or tumor volume greater or equal to 3000 mm^3. A total of 477 observations from 38 different animals were available for TGI modeling.

PK samples were collected 4 h after the first administration, 24 h after first, third, fifth and seventh injection and right before the six administration from 46 different animals.

Preclinical *in vitro* data (Papers II and III)

Different types of experiments aimed to investigate the increase in *in vitro* tumor cell killing when combining the bispecific costimulator FAP-4-1BBL with the CD3 TCB cibisatamab, compared to cibisatamab alone. The experimental set-up consisted of *in vitro* cell culture plates where tumor cells

(expressing CEA), fibroblasts (expressing different levels of FAP) and PBMCs (containing the T cells driving the *in vitro* tumor cell killing) were co-cultured.

Across different experiments that varied in levels of FAP expression, cibisatamab concentration, or FAP-4-1BBL concentration, both 4-1BB expression as well as *in vitro* tumor cell killing were measured. To establish the relationship between trimeric complex formation and *in vitro* tumor cell killing, cibisatamab at a fixed concentration of 2 nM was combined with 0, 0.01, 0.1, 1, 10, 100, 1000, and 10,000 nM of FAP-4-1BBL in an *in vitro* system with fibroblasts expressing either low (12,700 FAP/fibroblast) or high (92,000 FAP/fibroblast) levels of FAP.

To evaluate the changes in 4-1BB expression over time, T cells were subjected to continuous stimulation with cibisatamab (with or without FAP-4-1BBL) in the presence of tumor cells and FAP-expressing fibroblasts. Cibisatamab at 0, 0.2, 2, 20, 200, and 2000 nM, as well as 20 nM of cibisatamab combined with 1 nM of FAP-4-1BBL, were used to induce 4-1BB expression in an *in vitro* system with high (92,000 FAP/fibroblast) FAP expression. The 4-1BB expression was evaluated at 4, 21, 45, and 69 h after the start of the stimulation.

Simulated data (Paper III)

Simulations were conducted using the models developed in Paper II, and aimed to evaluate the effect of different FAP binding affinities on the expected increase in tumor cell killing when combining FAP-targeted 4-1BB costimulators with the CD3 TCB cibisatamab.

Across all simulations, the binding affinity to 4-1BB was considered identical to that of the lead FAP-4-1BBL molecule (K_D: 0.2 nM). Similarly, the relationship between trimeric complex formation on T cells and increase in tumor cell killing was also assumed to be that of the lead FAP-4-1BBL molecule.

A range of virtual molecules differing in their binding affinity to the FAP receptor was generated. In a further step, the expected clinical profiles of the lead FAP-4-1BBL molecule and a follow-up molecule with a ten-fold increase in FAP binding affinity were compared in 19 different solid tumor indications by simulating 1,000 virtual patients per indication differing in PK parameters and FAP expression.

Clinical PK data (Paper IV)

PK samples from two clinical phase I/Ib studies evaluating cibisatamab were available. Study BP29541 (NCT02324257) enrolled patients with advanced, CEA positive solid tumors. PK data from 143 patients was available from this study. Of these 143 patients, 27 patients received the anti-CD20 antibody obinutuzumab as pretreatment with the goal of depleting B cells and

diminishing ADA formation. No obinutuzumab PK samples were available. Study WP29945 (NCT02650713) evaluated cibisatamab in combination with the anti-PD-L1 inhibitor atezolizumab, and had cibisatamab PK data from 228 patients. No patient received obinutuzumab pretreatment in this study. In total, the dataset for modeling consisted of 11,341 samples from 371 patients with advanced solid tumors. The patients included in the PK analysis received at least one intravenous infusion with cibisatamab, either as a single agent with varying dosing frequencies (ranging from every week up to every three weeks) or in combination with atezolizumab at a dose of 1200 mg every three weeks.

Modeling

Modeling development using preclinical PK data

Model development for Paper I was conducted using the Monolix software (*Lixoft, a Simulations Plus Company*. Anthony (France)) version 2019R2 using the stochastic approximation expectation maximization (SAEM) algorithm. Different PK models (classic compartmental and simplified TMDD models) were explored. Parameters were assumed to be lognormally distributed.
Two different population PK models (*Model 1* and *Model 2*) were further developed to describe TYRP1-TCB concentrations. *Model 1* aimed to describe the PK of TYRP1-TCB as accurately as possible to serve as input for further PK/TGI model development. To capture the observed nonlinearity in volume of distribution versus dose, a two-compartmental PK model was fitted using data from the first administration to accurately estimate central volumes of distributions (Vc) for each treatment group. In a second step, the model was fit to all data to estimate the remaining PK parameters from a two compartmental model, while keeping Vc fixed from the first fit.

On the other hand, *Model 2* aimed to describe the PK of TYRP1-TCB (including the observed nonlinearity in volume versus dose) in a mechanistic manner that can serve to predict human exposure after translating the estimated parameters from mouse to human. For this purpose, a two-compartmental PK model with target-mediated drug disposition (TMDD) due to an easily accessible target in the central compartment was estimated using data from the first TYRP1-TCB administration. The inclusion of this easily accessible target allowed the reproduction of the observed nonlinearity of maximum concentration (Cmax) versus dose after the first administration. Receptor turnover or changes in total receptor amounts with tumor burden were not considered during model development. As it was not possible to estimate with precision both the accessible target and other PK parameters simultaneously, the volumes of distribution of the central and peripheral compartments and the inter-compartmental clearance were fixed to the typical values for IgG in mice available from literature (59 mL/kg, 60 mL/kg and 105 mL/day/kg,

respectively) (69). In a second step, the initial concentration of the accessible target in the central compartment was fixed to its estimated value (in the first step) before estimating the volume of distribution of the central compartment and the clearance on the full PK dataset. In this second step, the inter-compartmental clearance and the volume of the peripheral compartment were fixed to the typical mouse values for mAbs (105 mL/day/kg and 60 mL/kg, respectively).

Model development using preclinical TGI data

As observed by visualizing the change in tumor volume over time, the TGI model developed for Paper I needed to account for a delay between drug exposure and tumor shrinkage, a tumor shrinkage effect driven by TYRP1-TCB, and a time at which treatment effect is lost and the tumor regrows. Different TGI structural models were explored, including a monoexponential decay of treatment effect with time and the existence of two cell populations with different sensitivities to treatment. The final structural model selection was based on goodness-of-fit (GoF) plots, the precision of parameter estimates and Akaike Information Criteria (AIC). In the first step, the effect of anti-PD-L1 was evaluated by comparing the individual parameter estimates for the TYRP1-TCB monotherapy group at 2.5 mg/kg versus the same dose of the TCB plus anti-PD-L1 combination. Those parameters which showed differences among both groups were then estimated separately for the combination group.

Model development using *in vitro* data

A model framework was developed in Paper II to characterize the *in vitro* pharmacology of FAP-4-1BBL in combination with cibisatamab, as well as to elucidate the effect of different FAP expressions on the activity of FAP-4-1BBL.

One model was developed to quantify the change in 4-1BB receptors per T-cell over time after cibisatamab with or without FAP-4-1BBL. This model was a NLME model developed using Monolix version 2021R1. Lognormal distributions were assumed for all parameters, and the Fisher Information Matrix (FIM) was estimated with the stochastic approximation. When the standard deviation of the random effects could not be reliably estimated, it was fixed to a low value. The endpoint used for modeling was the number of 4-1BB receptors per CD8+ T-cell. Baseline 4-1BB expression levels (measured 4h after addition of cibisatamab or cibisatamab + FAP-4-1BBL) were assumed to be the ratio between the estimated synthesis (k_{in}) and degradation (k_{out}) rate constants.

As a higher FAP content in tumors has been shown to impair immune system activation in the tumor microenvironment (20), a model describing the

decrease in tumor cell killing with cibisatamab monotherapy as a function of the proportion of FAP-positive fibroblasts in the cell culture system was developed. The relationship between tumor cell killing with cibisatamab monotherapy and the proportion of FAP-positive fibroblasts was described using a generalized logistic model (*Equation 1*).

$$Tumor\ killing = Basal - \left(\frac{Maximum\ Decrease}{1+e^{-Sigmoidicity\times(Logit(\%\ of\ FAP)-midpoint)}}\right) \quad \textbf{(1)}$$

The model was developed using the logit-transformed proportion of FAP-positive fibroblasts as the independent variable. For the 0% and 100% FAP-positive fibroblasts conditions, a logit value of -7 and 7 (which would correspond to a percentage of 0.09% and 99.9%, respectively) was assumed. Lastly, the logit values were back-transformed to proportions and normalized to the 0% FAP-positive conditions.

Finally, a target engagement model describing the binding of FAP-4-1BBL to both FAP on fibroblasts and 4-1BB on T cells was developed and linked to the observed increase in tumor cell killing. In this model, free FAP-4-1BBL was assumed to bind independently and sequentially to the FAP receptor on fibroblasts and 4-1BB receptor on T cells. The binding rate constants of FAP-4-1BBL to free 4-1BB and FAP receptors were fixed to that calculated from *in vitro* experiments. This model assumes that all components (free bispecific antibody, free FAP and free 4-1BB) find themselves in a well-stirred and homogeneous system. In addition, this model considered the changes in 4-1BB expression over time, which were modeled as described above. The tumor cell killing model assumed that the FAP-4-1BBL trimeric complexes on T cells drive the increase in tumor cell killing in the cibisatamab + FAP-4-1BBL combination conditions compared to cibisatamab monotherapy.

Using this model and knowing the number of FAP receptors per fibroblast (available from *in vitro* measurements), the average number of trimeric complexes formed on T cells during the *in vitro* experiment (up to 120 h) was calculated. This number was then used as independent variable to fit an *Emax* model (*Equation 2*) relating the number of trimeric complexes formed to the observed increase in tumor cell killing with the cibisatamab and FAP-4-1BBL combination, compared to cibisatamab alone:

$$Tumor\ cell\ killing = \frac{(Maximum\ Increase - Baseline)\times TC^{Hill}}{TC^{Hill}+TC_{50}^{Hill}} + Baseline \quad \textbf{(2)}$$

where *TC* represents the number of trimeric complexes formed on T cells, TC_{50} represents the number of trimeric complexes on T cells required to achieve 50% of the maximum increase in tumor cell killing from baseline, and *Hill* represents the Hill coefficient of the increase in tumor cell killing as a function of trimeric complex formation on T cells.

Model development using clinical PK data

Model development for Paper IV was conducted in Monolix 2023R1 using the SAEM algorithm. Final model selection was based on the precision of parameter estimates, GoF plots, prediction-corrected visual predictive checks (pcVPCs) and the AIC. The M4 method (91) was used to model observations below the lower limit of quantification (LLOQ).

Due to observed ADA formation impacting the PK of cibisatamab in humans, model development was performed sequentially.

First, a base model was developed to describe cibisatamab's PK in patients with no ADA impact on drug exposure. A total of 116 patients were used to develop this model. Compartmental models with different elimination functions (linear, Michaelis-Menten, combined linear/Michaelis Menten, time-varying clearance) were tested. Once cibisatamab's PK was characterized in patients without ADA formation, the impact of ADA on cibisatamab's elimination was explored using all data available. ADAs were assumed to bind to cibisatamab only in the central compartment, with a 1:1 stoichiometry. Both free ADAs and the ADA-cibisatamab complex were assumed to be eliminated at the same rate. Different model structures were tested, including increased clearance over time as a result of neutralizing ADA formation, the Michaelis-Menten approximation to target-mediated drug disposition and an earlier-suggested semimechanistic model (92).

Finally, a mixture model was investigated on all available patient PK data. The mixture was implemented on the ADA formation constant parameter (estimated versus fixed to zero), and patient classification was based on a latent (unknown) covariate (93).

Covariates were tested for inclusion in the final model using the complete dataset. Sex, body weight and age were tested as potential covariates. Continuous covariates were implemented as per *Equation 3*, whereas categorical covariates (binary with values 0 or 1) were implemented as per *Equation 4*:

$$Par_i = \theta \times e^{\eta_i} \times e^{\beta \times \left(\frac{cov_i}{median(cov)}\right)} \quad \textbf{(3)}$$

$$Par_i = \theta \times e^{\eta_i} \times e^{\beta \; if \; cov_i = 1} \quad \textbf{(4)}$$

where Par_i represents the value of the parameter in the i^{th} individual, θ represents the typical value of the parameter, η_i represents the random effect of its associated θ for the i^{th} individual, cov_i represents the value of the covariate in the i^{th} individual, and β represents the estimate of the covariate effect on the parameter. Covariates were tested for inclusion in a stepwise fashion.

Translation from preclinical to clinical setting

Translation of parameters estimated from *in vivo* data

PK parameters estimated from mouse in Paper I were scaled allometrically to human assuming body weights of 0.02 and 70 kg, respectively. Volumes of distribution were scaled with an exponent of 1, while clearance and inter-compartmental clearance were scaled with an exponent of 0.92 (69). The concentration of target in the central compartment (driving the TMDD) was translated to human target concentration according to the interspecies differences in receptor expression and tumor burden. The interindividual variability in target expression per cell across different human samples (measured *in vitro*) was used as a surrogate of the interindividual variability in accessible target in human patients.

For the TGI model, in absence of data from a second nonhuman species to estimate the allometric exponent, parameters with units of time (such as *Time to tumor regrowth* or *Time to effect*) were scaled with an exponent of 0.25. Different growth rate constants for melanoma were retrieved from the literature (94), with the median being used for clinical simulations. The ratio between the growth rate constant and the maximum killing rate, between growth rate constants before and during tumor regrowth and enhanced efficacy of the combination between TYRP1-TCB and anti-PD-L1 were assumed to be conserved across species.

Interindividual variability was assumed to be conserved between species (with the exception of accessible target concentration in the central compartment for the PK model).

Translation of parameters estimated from *in vitro* data

In the case of the parameters estimated from *in vitro* data were generally considered to be conserved. It was, for example, assumed that in the clinic, the same number of trimeric complexes was required to achieve 50% of the maximum increase in tumor cell killing with FAP-4-1BBL in combination with cibisatamab (versus cibisatamab alone) as obtained from *in vitro* experiments.

The exception to this was the FAP expression, which was derived from immunohistochemistry (IHC) literature data (95). To transform the semi-quantitative IHC scores into a quantitative number of FAP receptors per fibroblast and the percentage of the tumor covered with fibroblasts, Monte Carlo simulations were used for both Paper II and Paper III. *Figure* 3 schematically represents the process used to derive quantitative FAP expressions from semiquantitative clinical data. In Paper II, FAP H-Scores were digitized for colon cancer and, in Paper III, for a total of 19 different oncology indications (95). These H-Scores were assumed to be lognormally distributed. Next, 5,000 virtual H-Scores per indication were simulated by sampling from a lognormal

distribution with the same location and dispersion as the original scanned H-Scores. Next, different percentages of high, medium and low FAP expression were assigned to each simulated H-Score, according to *Equation 5*:

$$H\text{-}Score = 3 \times High\ FAP\ area\ (\%) + 2 \times Medium\ FAP\ area\ (\%) + Low\ FAP\ area(\%) \quad \textbf{(5)}$$

Finally, a random number of FAP receptors per fibroblast was assigned to the high, medium and low FAP expressing areas by sampling from uniform distributions whose limits were defined based on *in vitro* data (300 to 1,000 for low, 1,000 to 7,000 for medium and 7,000 to 80,000 for high FAP expressions).

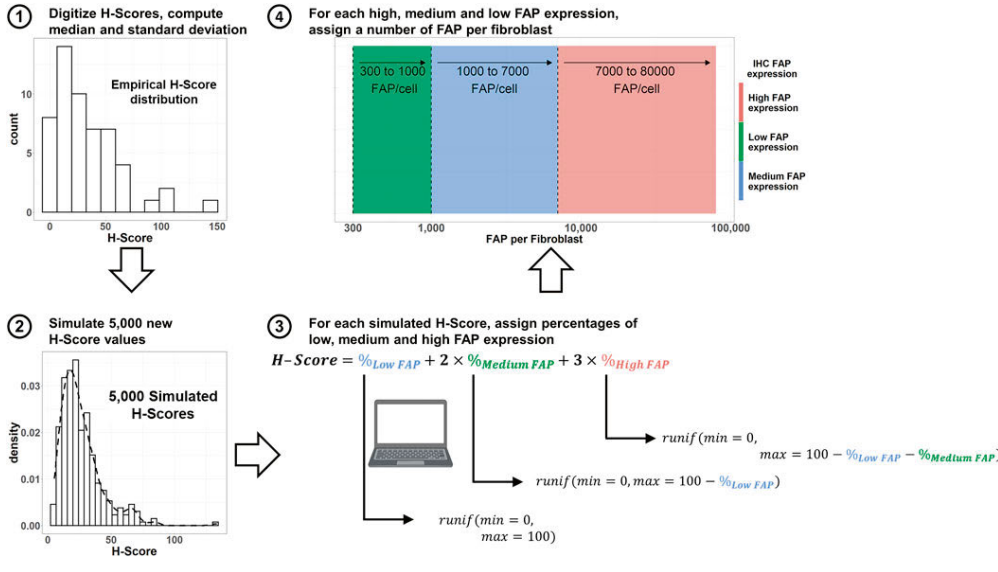

Figure 3. Workflow to simulate number of FAP receptors per cell and percentage of the tumor expressing with high, medium and low FAP-levels using digitized H-Scores from the literature. IHC: immunohistochemistry. FAP: Fibroblast Activation Protein. runif: random uniform distribution sample.

Simulation of untested scenarios

In vitro scenarios

In Paper III, several *in vitro* scenarios were tested *in silico* using virtual FAP-4-1BBL molecules differing in their FAP-binding affinity. The aim of these simulations was to evaluate both the minimum number of FAP molecules per fibroblast required to achieve 90% of the maximum pharmacological effect, as well as the range of bispecific antibody concentrations at which at least

50% of the maximum pharmacological effect could be achieved. To this effect, 4-1BB expression was always considered to follow the dynamics described in Paper II. In all cases, the relationship between trimeric complex formation and increase in tumor cell killing was assumed to be that of the original FAP-4-1BBL molecule.

To evaluate the minimum FAP expression required to achieve 90% of the maximum pharmacological effect, the concentration resulting in maximum trimeric complex formation was used for each virtual molecule. Then, FAP expression per fibroblast was varied and the expected increase in tumor cell killing was computed for each virtual molecule at each FAP expression.

To evaluate the range of concentrations at which at least 50% of the maximum pharmacological effect can be achieved, FAP expression was considered constant, with its value fixed to the median FAP expression in the colon cancer indication (an intermediate FAP-expressing tumor type).

Clinical scenarios

The expected clinical efficacy of TYRP1-TCB administered as a single-agent and in combination with anti-PD-L1 was simulated in 1,000 virtual patients per treatment group (monotherapy versus combination). Interindividual variability was considered both for PK as well as for PD parameters. An intravenous (IV) dose of 150 mg of TYRP1-TCB administered q3w for up to 400 days was used as efficacious dose. In line with the Response Evaluation Criteria In Solid Tumors (RECIST) guidelines (68), PFS, ORR and DOR were evaluated assuming that tumors were scanned every six, nine or twelve weeks. The RECIST-based efficacy metrics at each tumor scanning schedule were then compared to the efficacy metrics obtained using the full simulation data.

For Paper II, different clinical simulations were performed to evaluate the expected efficacy of FAP-4-1BBL in combination with cibisatamab at different doses and dosing schedules, as well as for different solid tumor indications. In all cases, the PK of FAP-4-1BBL was retrieved from published literature (96). Tumor distribution was modeled as a first-order distribution process from the central compartment assuming that tumor distribution did not affect amounts in the central compartment. Rate constants were selected based on in-house models and adjusted to represent either a 2.2:1 or a 10:1 plasma:tumor ratio.

To simulate the expected trimeric complex formation at different doses and dosing schedules with FAP-4-1BBL, 4-1BB expression was fixed to 80 receptors per T cell. The FAP expression was fixed to the median FAP expression in patients with CRC, and 1,000 virtual patients were simulated by random sampling from the FAP-4-1BBL population PK parameters. Trimeric complex formation in the tumor was simulated for this virtual patient population and for a range of FAP-4-1BBL doses between 1 and 120 mg administered qw,

q2w and q3w in combination with 100 mg of cibisatamab q3w. No other source of variability was considered for the evaluation of dose and scheduling.

Simulations were also performed to explore the impact of FAP expression in clinical activity when treating CRC patients with the combination of cibisatamab and FAP-4-1BBL. To do so, simulations were run for the same duration as the *in vitro* experiments (up to 120 hours). FAP-4-1BBL concentration-time course for the typical patient was simulated at a dose (2.75 mg) resulting in an average FAP-4-1BBL concentration in the tumor during the first 120 hours close to the FAP-4-1BBL concentration leading to maximum trimeric complex formation *in vitro*. From the free FAP-4-1BBL concentration in the tumor, trimeric complex formation was simulated using the developed target engagement model and assuming FAP expressions differing between patients. Next, tumor cell killing from cibisatamab monotherapy as a function of the percentage of FAP-positive fibroblasts was derived from the model relating the increase in FAP-expressing fibroblasts to the decrease in cibisatamab tumor cell killing. Lastly, the expected increase in tumor cell killing when cibisatamab is combined with FAP-4-1BBL compared to cibisatamab monotherapy as a function of trimeric complex formation with FAP-4-1BBL was considered the one observed *in vitro*.

Another relevant question answered by the means of stochastic simulations was the number of patients per dose cohort required to show a statistically significant difference in tumor cell killing when two different FAP-4-1BBL doses are combined with a single cibisatamab dose. To do so, tumor cell killing was simulated in a range of doses 165-fold lower and 350-fold higher compared to the dose that maximizes trimeric complex formation. For each of the doses, tumor cell killing was simulated for 1,000 virtual patients with variability in both PK parameters and tumor FAP expression. The expected effect at each dose was computed during the first week of treatment. To calculate the number of patients per dose needed to detect a difference between a given dose and the dose maximizing trimeric complex formation, different sample sizes (between 3 and 800 patients per dose) were evaluated. For each sample size, 100 permutation tests with 10,000 resamplings each were performed. The obtained p-values were then adjusted with the Benjamini-Hochberg method to correct for false positives occurring by chance. The number of patients per dose required to detect a difference between the tested dose and the dose that maximizes trimeric complex formation was defined as the minimum sample size at which statistical significance (adjusted p-value < 0.05 or p-value < 0.1) was achieved in at least 80% or 50% of the tests, respectively.

To simulate the expected efficacy of different *in silico* FAP-targeted 4-1BB costimulators across different solid tumor indications in Paper III, two different virtual molecules (FAP-binding affinity of 0.7 nM and 0.07 nM) were chosen. 4-1BB expression was fixed to be constant at 150 4-1BB receptors per T cell, and FAP expressions were simulated for 5,000 virtual patients per indication as detailed above. To simulate the best-case scenario, FAP-4-1BBL

exposure in the tumor was fixed to that resulting in maximum trimeric complex formation (and hence, maximum pharmacology) for each molecule. Next, the trimeric complexes formed were related to the expected fold increase in tumor cell killing using the model developed in Paper II.

Results

Models developed

PK model for TYRP1-TCB in mouse

After administration of the drug to the mouse xenografts, nonlinearity in volume of distribution of the central compartment versus dose was observed after the first administration. Data from subsequent administrations did not include sufficient information to conclude whether the nonlinearity persisted. For *PK Model 1*, the central volume of distribution (Vc) decreased with increasing doses, approaching a volume of 70 mL/kg at the highest dose. For *PK Model 2*, the assumption of TYRP1-TCB binding to an easily accessible target in the central compartment allowed reproducing the nonlinear Cmax versus dose.

TGI model for TYRP1-TCB

The TGI model schematically presented in *Figure 2* provided the best description of the data. The TGI model parameter estimates, their meaning, precision and inter-individual variability are presented in *Table 1*, together with their translation to human. The model allowed differentiating three different phases of the tumor kinetics: (i) a delay between drug exposure and the onset of tumor cell killing lasting an average of 1.26 days, (ii) the tumor shrinkage phase, where the drug exerted its tumor cell killing effect with an EC_{50} of 0.345 mg/L, and (iii) the tumor regrowth even in the presence of TYRP1-TCB exposure, which can be delayed up to a maximum of 11.5 days in monotherapy and a further 14.4 days in combination with anti-PD-L1. The time to transit between the delay between tumor cell killing and drug exposure and the tumor shrinkage phase is the estimated *Time to effect* parameter. During the tumor shrinkage phase, tumor cell killing followed a saturable *Emax* relation versus TYRP1-TCB concentration in the central compartment. The time to transit between the tumor shrinkage and tumor regrowth phase was defined as the *Time to tumor regrowth* parameter. In monotherapy, *Time to tumor regrowth* was related to TYRP1-TCB exposure via an *Emax* function with the shape determined by the estimated *Hill* coefficient. In this equation, the $Cav_{50,\ time\ to\ regrowth}$ parameter was the average concentration in the central compartment over the first two cycles, resulting in half of the maximum time to regrowth in monotherapy.

Tumor growth was determined by the estimated $k_{GROW,sensitive}$ parameter (exponential growth) until entering the tumor regrowth phase. During the tumor regrowth phase in monotherapy, the tumor growth rate increased with exposure or dose, with a maximum growth rate similar to what is estimated as tumor growth rate before the regrowth phase. A second identified beneficial effect of the combination with anti-PD-L1 was that the tumor growth rate during the regrowth phase was reduced to approximately one third of the maximal tumor growth for TYRP1-TCB in monotherapy.

Table 1. Parameter estimates for the tumor growth inhibition model developed in Paper I

Parameter	Description	Mouse estimate (RSE)	ω (RSE)	Human value
$k_{GROW,\ sensitive}$	Growth rate constant before tumor regrowth, day^{-1}	0.0605 (13)	0.52 (18)	0.0036
$k_{GROW,\ resistant\ MAX}$	Maximum growth rate constant after tumor regrowth, day^{-1}	0.061 (6)	0.1 (FIX)	0.0036
$k_{GROW,\ Combination}$	Growth rate constant after tumor regrowth in combination group, day^{-1}	0.0197 (30)	0.1 (FIX)	0.0012
$k_{DEATH\ Max}$	Maximum killing rate constant, day^{-1}	0.139 (12)	0.27 (39)	0.0083
EC_{50}	Concentration at which death rate is half of maximum, mg/L	0.345 (44)	0.1 (FIX)	0.345
$Time\ to\ regrowth_{MAX}$	Maximum time before tumor regrowth, days	11.5 (9)	0.16 (40)	88.5
$Time\ to\ effect$	Time before the start of drug effect, days	1.26 (19)	0.64 (22)	9.7
$Cav_{50\ time\ to\ regrowth}$	Average concentration for first two doses at which time to regrowth is half of maximum, mg/L	0.119 (43)	0.4 (FIX)	0.119
$Time\ to\ regrowth_{Comb.}$	Time before escape to treatment in combination group, days	14.4 (16)	0.33 (37)	110.8
$Cav_{50\ kGROW\ resistant}$	Average concentration for first two doses at which growth rate after escape to treatment is half of maximum, mg/L	0.0964 (45)	0.96 (36)	0.096
$Hill$	Hill coefficient for time to tumor regrowth as function of Caverage	1.53 (24)	0.1 (FIX)	1.53
a	Additive component of error model, mm^3	9.52 (17)	—	—
b	Proportional component of the error model, %	10.4 (11)	—	—

RSE: Relative Standard Error. ω: standard deviation of the random effects.

Model describing the change in 4-1BB receptor expression over time *in vitro*

4-1BB expression was found to be low at baseline (4 hours after stimulation start via the addition of cibisatamab with or without FAP-4-1BBL), to peak between 24-48 hours after stimulation start, and returned to baseline 72-96 hours after stimulation start. A semimechanistic model was developed to describe the time course of 4-1BB expression on T-cells, which increased with increasing cibisatamab concentrations and with addition of FAP-4- 1BBL to cibisatamab.

A *Signal* triggered by cibisatamab monotherapy (TCB) or cibisatamab in combination with FAP-4-1BBL (*Signal2*) was assumed to drive 4-1BB expression. The signal triggered by cibisatamab monotherapy followed an *Emax* relationship versus increasing cibisatamab concentrations, with an estimated EC_{50} of 16 nM. The signal from the cibisatamab combination was estimated as a single value (*Signal2*), as only one combination condition (20 nM of cibisatamab + 1 nM of FAP-4-1BBL) was tested. Both *Signals* were found to be short-lived and were modeled to instantly decrease to zero after an estimated timepoint of 16.2 hours. This time parameter was found to be independent of both cibisatamab concentration and FAP-4-1BBL costimulation. Then, seven transit compartments (T1–T7) best described (in terms of objective function value, residual unexplained variability, and precision of parameter estimates) the delay between administration of cibisatamab and peak in 4-1BB expression. The mean transit time was estimated to 28.6 hours.

Model describing the decrease in cibisatamab's tumor cell killing with increasing FAP-expressing fibroblasts

Cibisatamab monotherapy tumor cell killing was found to be at its maximum in the absence of FAP-positive fibroblasts in the co-culture system and decreased with increasing proportions of FAP-positive fibroblasts. Such a decrease could arise from the immunosuppressive effect of FAP-positive fibroblasts and needed to be accounted for when aiming to optimize the combination of FAP-4-1BBL and cibisatamab. This behavior was captured using *Equation 1*. The maximum decrease in tumor cell killing when the proportion of FAP-positive fibroblasts was increased was found to be 67%. Of note, the addition of FAP-4-1BBL to cibisatamab in this experiment also led to an increase in tumor cell killing which could be accounted for with the trimeric complex model and which was able to at least partially restore the lost effect of cibisatamab in monotherapy.

Trimeric complex formation on T cells and tumor cell killing increase *in vitro*

Trimeric complex formation between FAP-4-1BBL, T cells and FAP-positive fibroblasts was assumed to drive the increase in tumor cell killing when FAP-4-1BBL was combined with cibisatamab, as compared to cibisatamab monotherapy. In this model, both the proportion of FAP-positive fibroblasts, as well as the number of FAP receptors per fibroblasts were assumed to remain constant over time. The binding of free FAP-4-1BBL to the 4-1BB receptor or to the FAP receptor resulted in the formation of dimers. Both dimers could then bind to the other receptor, forming a trimeric complex. Dissociation of both the trimeric complex and/or the dimers to form their standalone entities could occur. In this model, receptor occupancy (both for FAP and 4-1BB receptors) was calculated as the percentage of receptors involved in the formation of either dimers or trimeric complexes. The number of trimeric complexes on both FAP per fibroblast and 4-1BB per T-cell was calculated as the percentage of receptors involved in trimeric complexes times the total number of receptors per cell. *Figure 4a* displays the observed increased tumor cell killing resulting from the addition of FAP-4-1BBL to 2 nM of cibisatamab when the fibroblasts in the co-culture system expressed high and low levels of FAP. A bell-shaped tumor cell killing versus FAP-4-1BBL concentration was observed at both the low and high FAP expression conditions, with the maximum increase in tumor cell killing occurring at around 1 nM of FAP-4-1BBL. Tumor cell killing increased nonlinearly versus trimeric complex formation. An *Emax* relationship (*Equation 2*) successfully linked the number of trimeric complexes formed on the T-cell surface with the increase in tumor cell killing (*Figure 4b*).

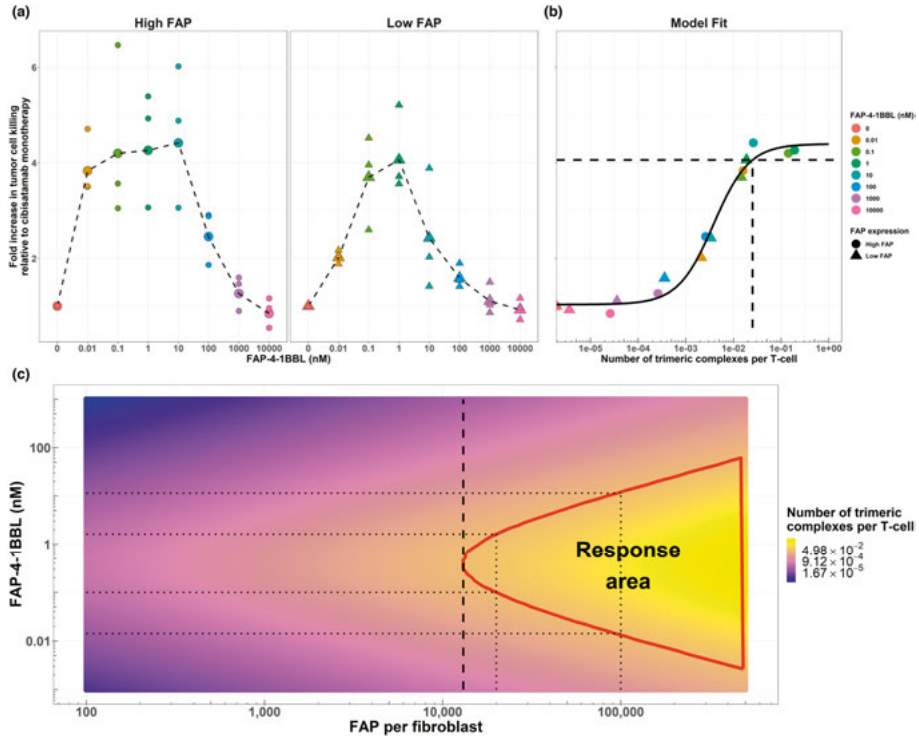

Figure 4. Increase in tumor cell killing when cibisatamab is combined with FAP-4-1BBL in the presence of fibroblasts expressing high and low levels of FAP **(a)**. Relationship between number of trimeric complexes on T cells and increase in tumor cell killing from *in vitro* experiments. Horizontal dashed line represents 90% of the maximum effect, and vertical dashed line represents the number of trimeric complexes on T cells leading to at least 90% of the maximum effect **(b)**. Impact of FAP-4-1BBL concentration and number of FAP receptors per fibroblast on trimeric complex formation. The *Response area* indicates the conditions under which at least 90% of the maximum effect can be achieved **(c)**.

PK model for cibisatamab in humans

When fitting the base model to the reduced dataset with patients without ADA-induced loss of exposure (see *Methods* section), a two-compartment model with clearance from the central compartment (*Equation 5*) best described cibisatamab's PK. Clearance was described as a combination of a constant component (*CLconst*) and a component decreasing mono-exponentially with time since first dose, involving *CLvar* and λ parameters. The typical maximum decrease in clearance and typical half-life of the decreasing clearance was 48% of the total initial clearance and 23 days, respectively. The full PK of cibisatamab (including both distribution and elimination, as well as the reversible binding to ADAs) is described in *Equation 6*. *Equation 7* describes the distribution of free cibisatamab to and from the peripheral compartment:

$$CL = CL_{const} + CL_{var} \times e^{-\lambda \times t} \quad \textbf{(5)}$$

$$\frac{d(A1)}{dt} = -\frac{CL+Q}{V1} \times A1 + \frac{Q}{V2} \times A2 - k_{on} \times ADA \times \frac{A1}{V1} + k_{off} \times Complex \quad \textbf{(6)}$$

$$\frac{d(A2)}{dt} = \frac{Q}{V1} \times A1 - \frac{Q}{V2} \times A2 \quad \textbf{(7)}$$

where *A1* and *A2*, *V1* and *V2* denote the amounts and volumes of distribution of the central and peripheral compartments, respectively, and *CL* and *Q* represent the central and inter-compartmental clearances.

For the full dataset, the ADA-driven loss of exposure was accounted for by including ADA formation, ADA binding to cibisatamab in the central compartment, and elimination of both free ADA and ADA-cibisatamab complexes in the central compartment. Only unbound cibisatamab was assumed to be distributed to the peripheral compartment. *Figure 5* schematically depicts the final structural model, together with a pcVPC and other GoF plots. Formation of ADAs was described by the k_{syn} parameter, which followed a bell-shaped relationship versus time (see *Equation 8* and *Figure 5*), and ranged from zero at start of treatment to k_{synMAX}. After reaching a maximum value, k_{syn} could decrease (which reflects transient ADA formation). Once formed in the central compartment, ADAs could bind to cibisatamab, forming a complex which could dissociate back to free ADAs and free cibisatamab. Both the free ADAs and the complex were assumed to be eliminated from the central compartment with rate constant $k_{out,\,ADA}$ (*Equations 9* and *10*):

$$k_{syn} = k_{synMAX} \times \frac{t^{Hill_{ADA}}}{t^{Hill_{ADA}} + T_{50,\ ksyn\ increase}{}^{Hill_{ADA}}} \times \left(1 - \frac{Max_{decrease} \times t^{Hill_{ADA}}}{t^{Hill_{ADA}} + \left(T_{50,\ ksyn\ increase} + T_{50ksyndecrease}\right)^{Hill_{ADA}}}\right) \quad \textbf{(8)}$$

$$\frac{d(ADA)}{dt} = k_{syn} - k_{out,ADA} \times ADA - k_{on} \times ADA \times \frac{A1}{V1} + k_{off} \times Complex \quad \textbf{(9)}$$

$$\frac{d(Complex)}{dt} = k_{on} \times ADA \times \frac{A1}{V1} - k_{off} \times Complex - k_{out,ADA} \times Complex \quad \textbf{(10)}$$

The final parameter estimates and their associated relative standard error (RSE) obtained by stochastic approximation are shown in *Table 2*. The model precision of parameter estimates showed no RSEs above 40%, and no major model misspecifications were apparent from observations versus predictions, residuals, and pcVPC plots. Large interindividual variability was estimated for many of the parameters related to ADA formation and elimination, as well as the ADA binding affinity to cibisatamab (k_{on}). Body weight was the only

covariate with a statistically significant impact on a PK parameter (central volume of distribution). The estimation of the exponent (β) for the impact of body weight on central volume of distribution (*Equation 3*) significantly improved model performance versus standard allometric scaling with a fixed exponent of 1.

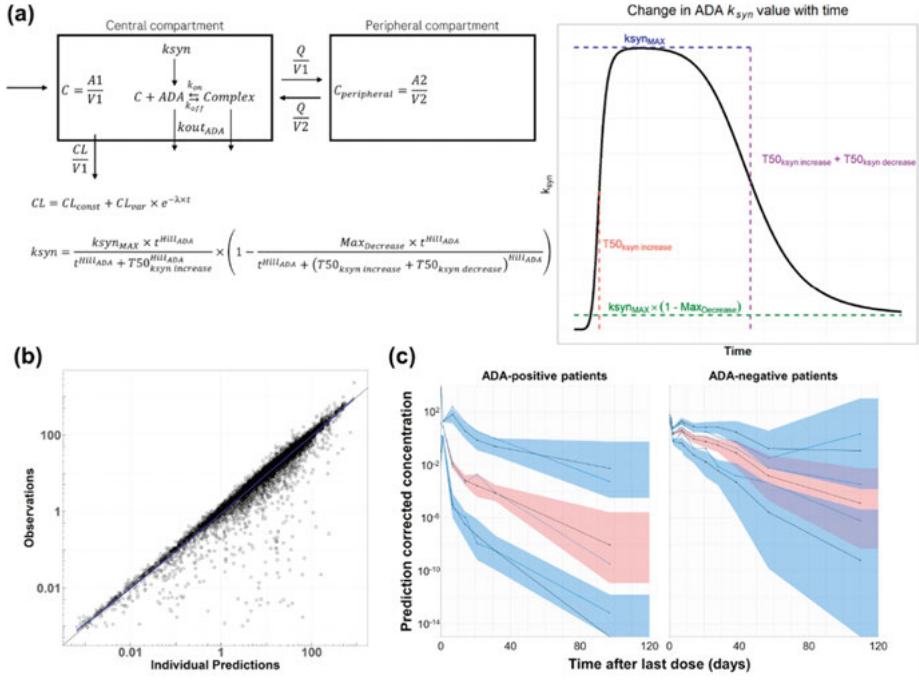

Figure 5. Schematic representation of the structural model developed to describe the PK of cibisatamab, as well as the formation of ADAs over time and their impact on cibisatamab's elimination **(a)**. Observations versus individual predictions **(b)** and prediction-corrected Visual Predictive Check (pcVPC) stratified by ADA status (positive versus negative) **(c)**.

The mixture model estimated the probability for a patient of belonging to the ADA-formation category to be 75%. No impact of patient covariates, dosing regimen or coadministration of atezolizumamb was identified for the probability of belonging to the ADA-formation or for the influence of ADAs on cibisatamab's exposure.

Table 2. Parameter estimates for the final population model describing cibisatamab's PK.

Parameter	***Description***	***Typical value (% RSE)***	***ω (% RSE) [% Shrinkage]***
V1	*Central compartment volume of distribution, L*	*3.87 (7)*	*0.31 (5) [-2.9]*
V2	*Peripheral compartment volume of distribution, L*	*2.76 (5)*	*0.69 (6) [23]*
CLconst)	*Constant clearance, L/day*	*1.11 (5)*	*0.85 (5) [12]*
CLvar	*Time-decreasing clearance at time=0, L/day*	*1.06 (6.2)*	*0.9 (5) [22]*
λ	*Rate of monoexponential decay for time-varying clearance, day⁻*	*0.0285 (14)*	*1.8 (7) [43]*
Q	*Inter-compartmental clearance, L/day*	*0.847 (5)*	*0.78 (7) [25]*
kon	*ADA-cibisatamab association rate constant, day×L/mg*	*56.3 (27)*	*3.73 (5) [25]*
koff	*ADA-cibisatamab complex dissociation rate constant, day^{-1}*	*0.1 (FIX)*	*0.1 (FIX) [—]*
$ksyn_{MAX}$	*Maximum ADA-formation rate constant, day^{-1}*	*64.9 (19)*	*2.62 (7) [35]*
$T_{50,\ ksyn\ increase}$	*Time at which ADA-formation constant is half of $ksyn_{MAX}$, day*	*49.3 (6)*	*0.74 (6) [5.3]*
$T_{50,\ ksyn\ decrease}$	*Time from $T_{50,\ ksyn\ increase}$ at which ADA-formation constant has decreased to half of its maximum decrease value, day*	*287 (38)*	*3.06 (11) [58]*
$Max_{Decrease}$	*Maximum decrease (as proportion) in ADA-formation constant over time*	*0.94 (0.1)*	*0.1 (FIX) [—]*
$Hill_{ADA}$)	*Hill coefficient of ADA-formation constant and time function*	*6.72 (5)*	*0.69 (6.5) [28]*
$k_{out,\ ADA}$	*ADA and complex elimination rate constant, day^{-1}*	*0.852 (27)*	*3.13 (9) [51]*
Corr(V1, CLconst)	*Correlation coefficient between V1 and CLconst*		*0.589 (9)*
Corr(V2, Q)	*Correlation coefficient between V2 and Q*		*0746 (6)*
WT on V1	*Weight effect in volume of distribution of the central compartment*	*0.511 (12)*	
p(ADA)	*Probability of belonging to group with ADA formation*	*0.748 (3)*	
p(No ADA)	*Probability of belonging to group without ADA formation*	*0252 (—)*	
b	*Proportional residual error, %*	*33.6 (1)*	*[6]**

*RSE: Relative Standard Error. *Epsilon-shrinkage (expressed as a percentage), calculated as 1-sd(IWRES), where sd denotes standard deviation and IWRES denotes Individual Weighted Residuals.*

In vitro simulations

FAP expression per fibroblast versus increase in tumor cell killing

Figure 4c displays the expected trimeric complex formation as a function of FAP-4-1BBL concentration and number of FAP receptors per fibroblast. Of note, trimeric complex formation follows the previously discussed bell-shaped response versus bispecific antibody exposure, whereas it increased almost linearly versus number of FAP receptors per fibroblast (while keeping the bispecific antibody concentration fixed). When simulating the number of trimeric complexes formed at different FAP-4-1BBL exposures and FAP expression, the minimum number of FAP receptors per fibroblast to achieve 90% of the maximum tumor cell killing was about 13,000 FAP/fibroblast.

To further extend this workflow, the minimum number of FAP receptors per fibroblast to achieve 90% of the maximum tumor cell killing was evaluated as a function of FAP binding affinity for different virtual FAP-4-1BBL molecules. In a next step, this number was compared to the expected FAP expression across 19 different oncology indications. From *Figure 6* it can be noted how increasing FAP binding affinity decreased the number of FAP receptors per fibroblast required to achieve at least 90% of the maximum effect. In turn, the percentage of the patient population above this threshold increased. *Figure 6* also shows that certain indications (like kidney cancer) are expected to express too low FAP/fibroblast numbers to achieve clinically meaningful pharmacology even if FAP binding affinity is markedly increased.

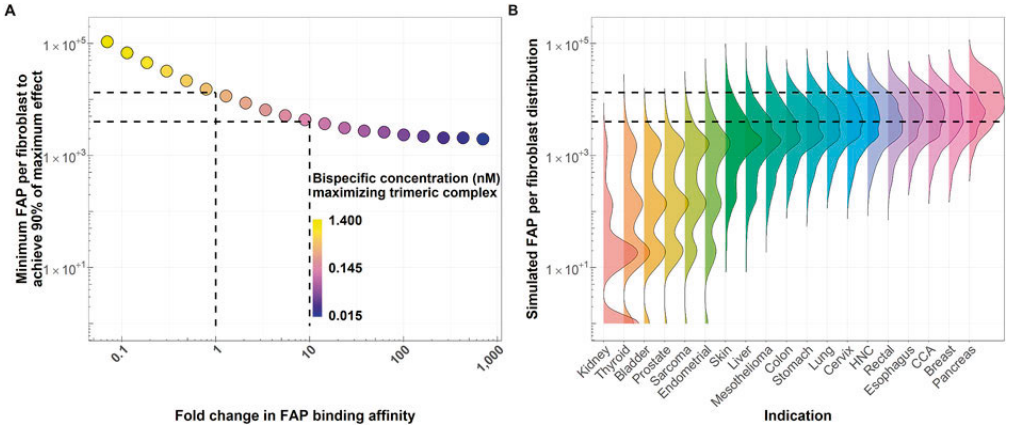

Figure 6. (A) Number of FAP per fibroblast required to achieve at least 90% of the maximum effect with virtual FAP-4-1BBL molecules differing in their binding affinity to FAP. Dashed lines indicate the number of FAP/fibroblast required to achieve 90% of the maximum effect with a reference molecule (same binding affinity as FAP-4-1BBL) and a molecule with an enhanced 10-fold increase in FAP binding affinity. **(B)** Simulated average number of FAP receptors per fibroblast in different solid tumor indications. Dashed lines represent the number of FAP per fibroblast required to achieve 90% of the maximum effect with the reference molecule and the molecule with the 10-fold increase in FAP-binding affinity.

Range of active exposures versus binding affinity

The range of concentrations at which at least 50% of the maximum pharmacological effect could be achieved was evaluated as a function of FAP-binding affinity. *Figure 7* shows the conditions (in terms of bispecific antibody concentration and FAP-binding affinity) at which at least 50% of the maximum pharmacological effect was predicted to be achieved at an FAP expression equal to the typical colon cancer patient. The range of bispecific antibody exposures leading to 50% of the maximum pharmacological effect increased with increasing FAP-binding affinity. For instance, a range of concentrations between 0.1 and 1.2 nM with the reference molecule would allow at least 50% of the maximum pharmacological effect, compared to a range of 0.01–2 nM for a molecule with a 10-fold higher binding affinity on the FAP receptor. The increase in exposure range leading to at least 50% of the maximum pharmacological effect was due to increased trimeric complex formation with higher FAP-binding affinities. Not only does the range of exposures increase, but also the number of trimeric complexes formed at a given bispecific antibody concentration. For example, the number of trimeric complexes per T cell would be 0.005 for the reference molecule and 0.016 for the molecule with a 10-fold increase in FAP-binding affinity (3.2-fold increase). Lastly, molecules with FAP-binding affinities 1.7-fold lower than the reference molecule could not achieve 50% of the maximum pharmacological effect regardless of bispecific antibody exposure.

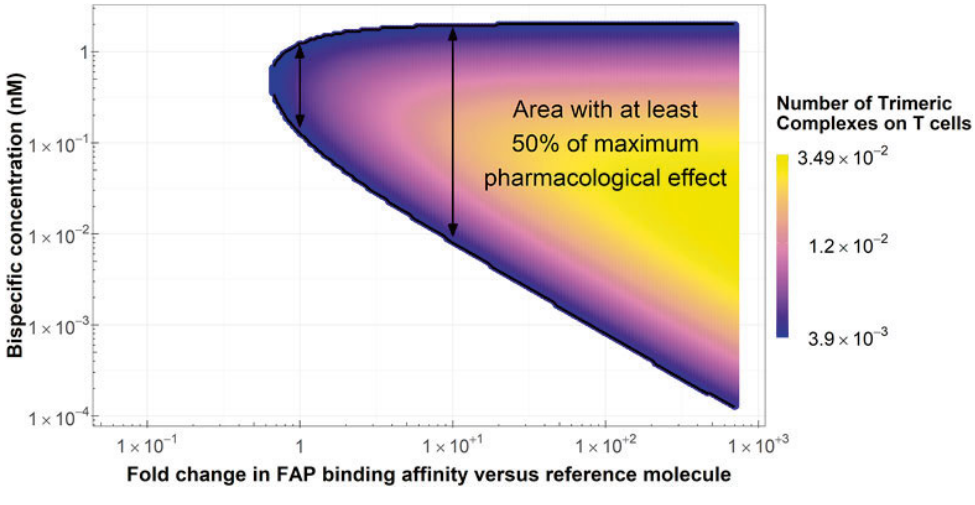

Figure 7. Conditions (in terms of bispecific antibody concentration and FAP-binding affinity) at which at least 50% of the maximum pharmacological effect can be achieved. Vertical arrows represent the reference molecule (left) and a molecule with a 10-fold increase in FAP-binding affinity.

Clinical simulations

Expected efficacy of TYRP1-TCB with or without anti-PD-L1 in advanced melanoma patients

After simulating the expected tumor growth inhibition profiles for 1,000 virtual patients treated with TYRP1-TCB single agent or TYRP1-TCB in combination with anti-PD-L1, different RECIST-derived metrics were summarized in *Table 3*.

Table 3. Clinical endpoint summary for 150 mg q3w of TYRP1-TCB monotherapy and combination with anti-PD-L1. For relevant endpoints, data is presented as median (5^{th}-95^{th} percentile).

	TYRP1-TCB monotherapy				***TYRP1-TCB combination with anti-PD-L1***			
End-point	***True value in simulation***	***Predicted observed value at each scanning frequency***			***True value in simulation***	***Predicted observed value at each scanning frequency***		
		q6w	*q9w*	*q12w*		*q6w*	*q9w*	*q12w*
ORR (%)	*27.2*	*12.6*	*7.8*	*6.1*	*41.6*	*35.2*	*30.8*	*27.8*
DOR (days)	*72 (50-103)*	*84 (84-126)*	*126 (63-126)*	*84 (84-168)*	*197 (153-289)*	*210 (168-NE)*	*252 (189-NE)*	*252 (168-NE)*
PFS (days)	*143 (28-172)*	*175 (49-217)*	*196 (70-196)*	*175 (91-259)*	*265 (28-358)*	*301 (49-NE)*	*322 (70-NE)*	*343 (91-NE)*

ORR: Objective Response Rate. PFS: Progression-free survival. DOR: Duration of response.

In line with the results observed in mice, the simulated expected efficacy of TYRP1-TCB in combination with anti-PD-L1 exceeded that of TYRP1-TCB in monotherapy. This beneficial effect of the combination resulted in increased ORR (27% versus 42%), DOR (72 versus 197 days) and PFS (143 versus 301 days). The benefits of the combination of TYRP1-TCB with anti-PD-L1 are observed regardless of the tumor scanning frequency.

Table 3 also demonstrates that a more frequent clinical scanning provides the closest assessment of the true patient response (*i.e.* the lowest discrepancy between the result under that tumor scanning, and the result obtained with the higher-granularity simulation). For instance, ORR in monotherapy was 12.6% vs. 6.1% when tumor evaluation was performed every 6 vs. 12 weeks, whereas the true simulated value is 27.2%. In contrast, in the combination group, 27.8 to 35.2% (12 weeks versus 6 weeks scan frequency) of the patients would be classified as responders, compared to 41.6% who actually responded.

The median DOR observed under different tumor-scanning frequencies ranged from 84 to 126 days and from 210 to 252 days for the TYRP1-TCB monotherapy and TYRP1-TCB plus anti-PD-L1 combination respectively,

versus 72 and 197 days DOR predicted from the translational model, respectively. In this example, following the RECIST recommendation leads to overestimating the DOR between 12 and 60 days, depending on the scanning frequency and the addition or not of anti-PD-L1 as a combination partner. DOR is overestimated across all the scanning frequencies (as compared to the simulation) due to the failure to detect the true nadir (minimum recorded tumor value while on study), from which the 20% increase triggering the progression event is calculated. As the true nadir is frequently achieved between two tumor scans, the true progression frequently requires a smaller absolute increase in tumor size than expected when the nadir is determined from the scans. Similar results were observed for PFS, where the median under different tumor-scanning frequencies ranged between 175 and 196 days and 301 to 343 days for the TYRP1-TCB monotherapy and TYRP1- TCB plus anti-PD-L1 combination, respectively, versus the simulated PFS of 143 and 265 days. In this example, following the RECIST recommendation leads to a delay in identifying progression of between 30 and 72 days, depending on the scanning frequency and the addition or not of anti-PD-L1 as a combination partner.

Clinical dose selection with FAP-4-1BBL

In order to select the clinical doses and dosing schedules leading to the maximum pharmacological effect with FAP-4-1BBL, trimeric complex formation (and, specifically, the area under the trimeric complex formation curve versus time) was used as a surrogate. *Figure 8* shows the area under the trimeric complex curve simulated for 30 weeks in the tumor at different doses and dosing schedules, with interindividual variability being considered only for FAP-4-1BBL plasma PK. Trimeric complex formation was evaluated under two different plasma:tumor distribution ratios of 2.2 and 10. As observed from *in vitro,* trimeric complex formation with FAP-4-1BBL in the clinic was expected to follow a bell-shaped response versus dose.

The dose leading to the largest median area under the trimeric complex curve in the tumor (solid line) ranged from 3 mg for a q.w. schedule assuming a 2.2 plasma:tumor ratio, to 67 mg for a q3w schedule assuming a plasma:tumor ratio of 10. Of note, trimeric complex formation was higher the more frequent the dosing schedule (maximum median trimeric complex formation of 87 in the q.w. schedule, versus 63 for the q3w schedule).

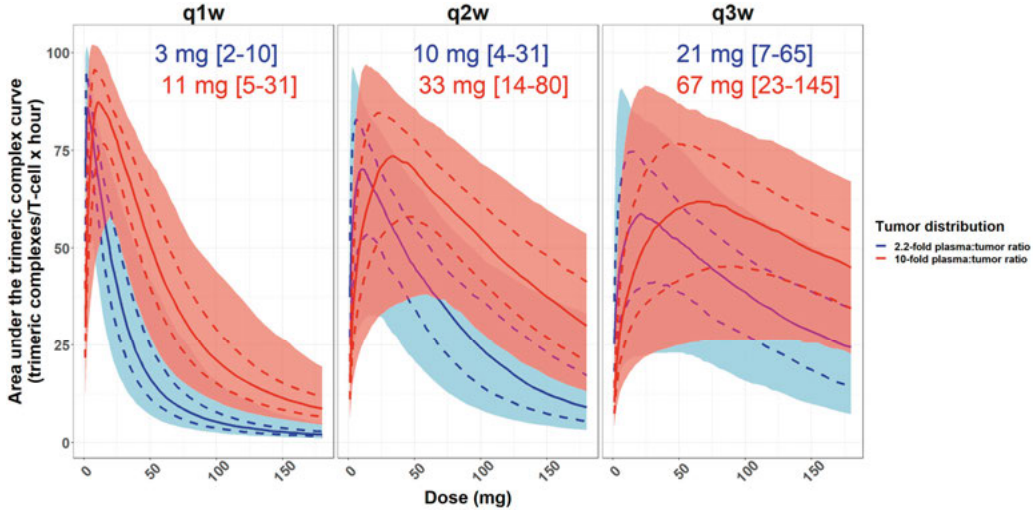

Figure 8. Trimeric complex formation at different doses, schedules, and plasma:tumor distribution ratios. Solid lines represent the median of 1,000 virtual patients. Dashed lines represent the 25th-75th percentiles, and shaded areas represent the 5th-95th percentiles. Text annotations represent the dose at which trimeric complex formation is maximum and within brackets, the dose range at which trimeric complex formation drops no more than 20% from the maximum.

The predicted range of doses at which FAP-4-1BBL resulted in marked trimeric complex formation was wide. Doses between as low as 2 mg and as high as 145 mg would lead to less than a 20% drop from the maximum median trimeric complex formation. Similarly, although only interindividual variability on PK parameters was considered for this simulation, the expected variability in trimeric complex formation at a given dose is also expected to be high and to overlap with doses less than threefold apart.

FAP as a biomarker to predict clinical activity with FAP-4-1BBL in combination with cibisatamab

FAP-positive fibroblasts in the tumor was predicted to lead to more trimeric complex formation *(Figure 9*). In turn, this leads to a greater fold increase in tumor cell killing, as compared to cibisatamab monotherapy. This highlights that patients are expected to obtain some degree of benefit from FAP-4-1BBL addition to cibisatamab. However, as cibisatamab tumor cell killing decreases with increasing proportions of FAP-positive fibroblasts, in absence of comparative data with cibisatamab monotherapy, the percentage of FAP-positive fibroblasts in the tumor will not be predictive of the overall response to the combination treatment with cibisatamab and FAP-4-1BBL (right-most plot).

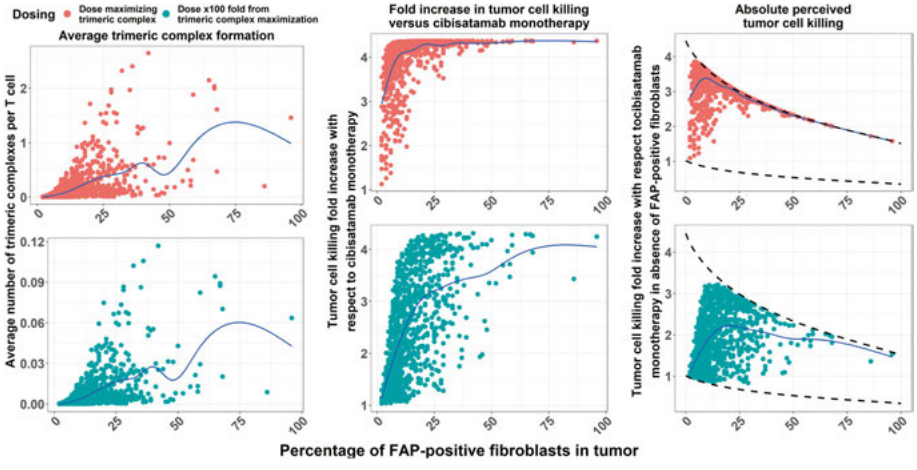

Figure 9. Trimeric complex formation with FAP-4-1BBL (left), associated increase in tumor cell killing when combining FAP-4-1BBL and cibisatamab versus cibisatamab monotherapy (middle), and absolute perceived tumor cell killing after accounting for the decrease in cibisatamab's effect with increasing FAP expression. Each point represents a virtual patient, treated with a dose maximizing trimeric complex formation (red) or a dose 100-fold higher (blue).

Number of patients per dose cohort to observe a significant difference in theoretical tumor cell killing

A clinical trial of more than 100 patients per arm was predicted to be needed to separate the tumor cell killing for doses between 0.35 and threefold away from the dose maximizing trimeric complex formation, while a statistically significant difference in tumor cell killing was demonstrated for the dose maximizing the trimeric complex formation and a dose 10-fold higher in a clinical trial with about 35 patients per dose arm.

Under less stringent criteria (alpha level 0.1, 50% of power), a trend toward superiority could be detected with 15 patients per dose level when comparing the dose maximizing the trimeric complex formation and a dose about 10-fold higher. The high number of patients required to discriminate two doses with a 3-fold difference in dose highlights the challenge of dose selection based solely on emerging clinical data, emphasizing the advantages of an integrative modeling and simulation approach.

Increase in tumor cell killing as a function of FAP binding affinity

Across all indications, the virtual bispecific costimulator with 10-fold higher FAP-binding affinity (blue) results in increased percentage of the maximum pharmacological effect, compared to the reference molecule (*Figure 10*). The

largest increase in percentage of the maximum pharmacological effect was found for the endometrial cancer indication (median pharmacological effect of 24.6% and 55.8% for the reference and the enhanced binding affinity molecules, respectively). Interestingly, indications with low FAP levels of expression did not show a large increase in pharmacological effect when increasing FAP binding affinity 10-fold, indicating that even higher binding affinity may be required if FAP is to be pursued as targets in these indications. Conversely, indications with high level of median FAP expression (and hence, marked pharmacology already with the original molecule) could achieve notable increases in the maximum effect with the enhanced molecule. This increase is mainly driven by the lower FAP-expressing patients within that population, who are not expected to achieve much trimeric formation with the reference molecule, but could benefit greatly from the enhanced binding affinity molecule.

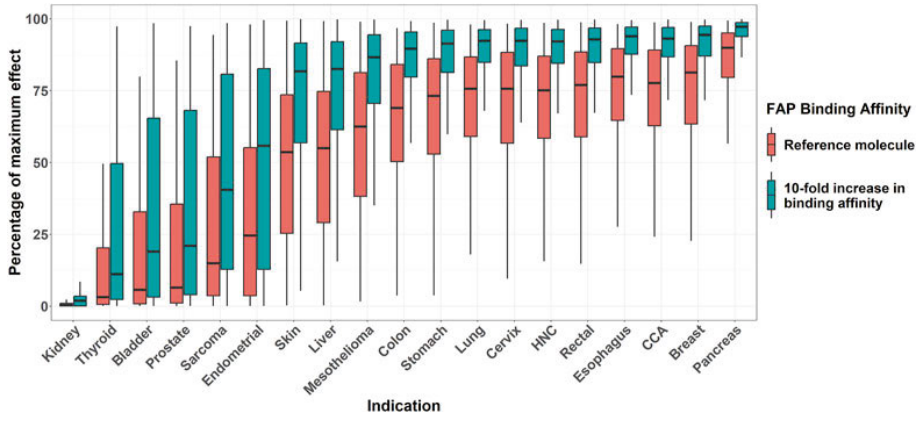

Figure 10. Percentage of the maximum effect achieved with the reference molecule and a molecule with a 10-fold increase in binding affinity across different solid tumor indications.

ADA-driven loss of exposure with cibisatamab

The simulations did not indicate an impact of evaluated patient covariates, dose or dosing schedule on ADA formation and exposure loss, except for pretreatment with the CD20-targeted antibody obinutuzumab (52% of patients developing ADAs according to the model versus 78% in the non-pretreated group). Furthermore, the average exposure loss for those patients pretreated with obinutuzumab who developed ADAs was 25%, compared to 54% average exposure loss for those patients developing ADAs without obinutuzumab pretreatment.

ADA titers were qualitatively correlated with the model-predicted exposure. A clear heterogeneity in PK profile and change in ADA titer over time was noted (*Figure 11*).

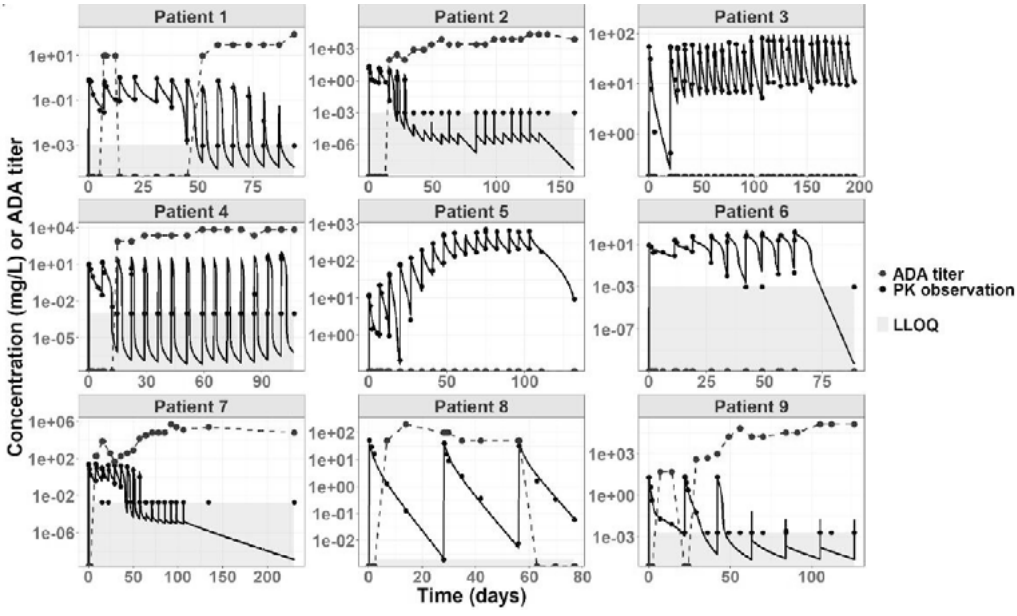

Figure 11. Representative examples of measured ADA titers (blue) with individual PK profiles and PK observations (black circles). Grey area represents the lower limit of quantification (LLOQ).

For instance, *Patient 4* showed an increase in ADA titer around day 15 after start of treatment, which approximately matched the time where the PK profile starts showing signs of ADA-driven exposure loss. Conversely, *Patient 6* and *Patient 8* illustrate how ADA titers were not always predictive of exposure loss (ADA titers are detectable in *Patient 8* without signs of loss of exposure, whereas *Patient 6* shows a PK profile compatible with ADA-driven loss of exposure, despite all the ADA samples testing negative). In fact, up to 29 patients in the monotherapy study of cibisatamab and 20 patients in the combination study of cibisatamab plus atezolizumab had no quantifiable ADA titers while on study despite displaying loss of exposure according to their observed PK and model-derived individual PK profiles. For these patients, however, the model-predicted loss of exposure was on average 18.5% and 24%, tending to be lower than that observed in the total ADA-positive population (approximately 50%).

Discussion

Developing new cancer immunotherapy combinations requires the integration of data from preclinical experiments, the translation of their insights to the clinical setting and a quantitative understanding of the interplay between drug exposure, PD effect and tumor biology. This thesis explored how to translate insights from preclinical experiments into actionable clinical strategies by using mathematical modeling and simulation. Furthermore, the *in silico* approach presented can facilitate the design of optimized therapeutic candidates by integrating knowledge from previous drug candidates and disease biology (*e.g.* target expression in the patient population of interest). Together, these methodologies can support the design of oncology therapies, clinical trials and patient population selection.

Translating preclinical TGI to clinical outcomes

In Paper I, a TGI model was developed describing the tumor kinetics observed in mice xenografts treated with TYRP1-TCB as single agent or in combination with anti-PD-L1. It was assumed that a similar profile as observed in mice (transient drug effect followed by tumor regrowth, which can be delayed by combining TYRP1-TCB with anti-PD-L1) would be observed in humans.

The expected RECIST-based results in monotherapy, even at a TYRP1-TCB dose in range with the estimated EC_{90}, would likely warrant no further development of the molecule. At the most frequent tumor scanning interval (q6w), the ORR was found to be only 12.6%, which falls below the benchmark set by other immunotherapies approved and under investigation for relapsed melanoma (97). Conversely, the combination of TYRP1-TCB and anti-PD-L1 would be (under the same assumptions) associated with a 35.2% ORR, more than 10 months of median PFS, and 7 months of median DOR. The results of the combination do warrant, in consequence, further research and evaluation in clinical trials.

However, it is common that, in oncology drug development, candidate molecules are first investigated as a single agent and later, only if single-agent activity has been demonstrated (*i.e.* response rate of around 20%), are they tested in combination. The findings of Paper I suggest that this strategy would result in the premature termination of TCBs with tumor growth inhibition

profiles like what was observed for TYRP1-TCB (transient tumor shrinkage followed by fast tumor regrowth in monotherapy, but delayed tumor shrinkage and reduced tumor regrowth rate in combination). Importantly, it was shown how this shortfall can be anticipated by integrating preclinical data in a modeling network. Then, after parameter translation, clinical simulations can be conducted to design (even if only at a high-level) the most successful development strategy.

For molecules like TYRP1-TCB, which may be expected to be markedly more efficacious in combination than in monotherapy, combination clinical trials should not be gated on RECIST-based efficacy metrics from single-agent studies. Instead, we proposed that these products are researched in combination with other cancer immunotherapies that may enhance their properties as early as possible.

Nevertheless, the proposed approach is not without limitations, which need to be carefully considered when designing the most appropriate strategy for each molecule. Firstly, the model was developed using mouse data, and the translation of the model to clinic (and its derived simulations) have not been contrasted against clinical data. However, tumor regrowth similar to what was predicted for TYRP1-TCB single-agent has already been observed in the clinic with other TCBs (44,55). Nevertheless, due to the intrinsic limitations of clinical TGI data (tumor scans every six weeks at best, patients dropping out from study after disease progression), the development of a model as complex as the one developed to explain TYRP1-TCB's TGI profile may not be feasible. This highlights the value of incorporating preclinical insights into clinical development strategies.

Furthermore, the proposal of combining molecules like TYRP1-TCB as early as possible in development is based on expected surrogate endpoints (ORR, PFS and DOR). In practice, overall survival (OS) is the endpoint of highest interest in oncology research. In the case of cancer immunotherapies, increased response rates have not always translated into improved OS (98), and improvements in OS have been noted even without a higher ORR (99). Whether the development of oncology drugs without single-agent activity is warranted has also been called into question, given that in general they do not improve OS (albeit this analysis did not include cancer immunotherapies) (100).

In summary, the development of this model aided with the translation of a complex dose-response from mouse to human. Additionally, it quantitatively characterized the benefit of the combination (increase in time to tumor regrowth and decrease in tumor regrowth rate), which when translated into clinical endpoints suggests an optimized development strategy for TYRP1-TCB and other TCBs displaying similar tumor regrowth profiles. It is therefore recommended to consider development as part of combination therapies as early as possible, with such combination trials not being solely gated on early RECIST-based efficacy assessment of TCB monotherapy trials.

Deconvoluting the effect of drug exposure and target expression

In Paper II, a workflow using *in vitro* data and mathematical modeling and simulation was developed to recommend a range of doses worth exploring in the clinic with FAP-4-1BBL. Furthermore, the potential use of a biomarker (FAP-positive fibroblasts in tumor biopsies evaluated by IHC) to guide patient selection with FAP-4-1BBL was also explored, as was the expected number of patients per dose cohort to differentiate clinical activity between two doses.

As previously discussed, TCBs for solid tumor treatment may unleash their full potential when used in combination with other cancer immunotherapies. If a TCB is to be developed in combination, a key question to be tackled is how to select the doses of each agent. In the case of the combination of cibisatamab and FAP-4-1BBL, the two main questions were: which cibisatamab exposures trigger sufficient 4-1BB expression on T cells (and how does this expression vary over time), and how to consider the bell-shaped exposure-response observed preclinically with FAP-4-1BBL when selecting clinical doses.

The semimechanistic model developed to describe 4-1BB expression over time when T cells are stimulated with cibisatamab described not only when is the maximum expression of 4-1BB reached, but also quantified the relationship between cibisatamab exposure and the increase in 4-1BB expression. From this information, it could be inferred that concomitant administration of both drugs would allow FAP-4-1BBL exposure at a time where 4-1BB expression is expected. Furthermore, the model also suggested that a relatively wide range of cibisatamab exposures is expected to result in sufficient 4-1BB expression on T cells for FAP-4-1BBL to exert its costimulatory effect.

With regards to the exposure-tumor cell killing relationship observed from *in vitro* data, the target engagement model was capable of deconvoluting the effect that both FAP-4-1BBL exposure and FAP expression on fibroblasts showed on tumor cell killing. By calculating the number of trimeric complexes formed with FAP-4-1BBL under different conditions, an *Emax*-like relationship between trimeric complexes and tumor cell killing could be established.

The performed simulations anticipated that, given the expected FAP expression variability in the clinic, observing a clear exposure-response relationship in patients may not be straightforward (due to the role that target expression plays in trimeric complex formation). This is in line with what has been observed clinically with other 4-1BB costimulators (101).

If target expression is expected to play an important role in trimeric complex formation (and, as a result, in pharmacological effect), it is relevant to explore whether its expression can be used to guide patient selection or, at least, provide a stratification factor during clinical development. To do so, it was necessary to acknowledge that, in the clinic, FAP expression cannot be measured with as much granularity as in the *in vitro* experiments used for

model building. To account for this, a workflow was developed where H-Scores retrieved from the literature were transformed into quantitative values of number of FAP receptors per fibroblast. This allowed simulating the expected trimeric complex formation and associated increase in tumor cell killing for each of these H-Scores. Although higher FAP expressions result in higher trimeric complex formation with FAP-4-1BBL, they also result in decreased cibisatamab activity. When both aspects were considered together, and the expected tumor cell killing was visualized versus percentage of FAP-positive fibroblasts in the tumor, no clear trend could be observed. These results suggest that, in a single-arm study, FAP expression quantified with the current IHC techniques would not provide sufficient granularity to enable patient selection.

Because the FAP-4-1BBL exposure that maximizes trimeric complex formation is independent from receptor expression (102,103), dose selection with FAP-4-1BBL and similar bispecific costimulators can be done independently from target expression. Our results suggest that just by considering interindividual variability on PK parameters, the range of doses at which marked trimeric complex formation is expected is wide. However, in keeping with the *in vitro* data and the expected bell-shaped relationship of trimeric complex formation versus exposure, trimeric complex formation is anticipated to decrease at too high doses. This highlights the importance of not following an MTD approach when aiming to select the Recommended Phase 2 Dose (RP2D), but rather exploring a range of doses to characterize the dose-exposure-response, as recently discussed by the FDA (76). Instead, a modeling and simulation approach informed using preclinical data can provide a range of doses where trimeric complex formation is expected to be maximized.

Given the expected variability in trimeric complex formation even at the same dose (arising both from interindividual variability in PK, as well as from differences in target expression), we investigated the number of patients per dose cohort required to achieve statistical significance when comparing a given dose with the dose maximizing trimeric complex formation. The results suggest that a large number of patients (approximately 35 patients) per dose would be required if both doses are less than three-fold apart. This number has to be considered as underestimated as these simulations have not considered additional variability sources (such as T cell activity, tumor burden in patients, or the dynamics of tumor shrinkage). Although statistical superiority is not a requirement for dose optimization in oncology drug development, these results highlight the difficulties of understanding dose-exposure-response solely based on emerging clinical data. Furthermore, randomized, controlled trials (RCTs) with TCBs comparing two different doses with 80 patients per arm and a ten-fold difference in doses have already been conducted to pursue optimal dose selection (104).

In summary, the development of these models and their use in simulations allowed clarifying the contribution of drug exposure and receptor expression

to the observed exposure-tumor cell killing relationship *in vitro*. With this, a range of doses maximizing trimeric complex formation in the clinic was proposed and, as a last step, an estimation of the number of patients required to conduct dose-finding in the clinic if no modeling approaches were to be used was provided. Lastly, a threshold in the number of FAP per fibroblast to achieve 90% of the maximum effect when combining FAP-4-1BLB with cibisatamab was established, and the use of FAP-positive fibroblasts in tumor biopsies evaluated by IHC as potential biomarker was explored to aid with patient selection.

In silico design of refined bispecific costimulators

As explored in Paper II, bispecific costimulators are expected to exhibit a bell-shaped dose/exposure-response. Furthermore, target expression is expected to impact trimeric complex formation and, as a result, pharmacology. In consequence, patients with too low FAP expression may not achieve sufficient number of trimeric complexes to benefit from the therapy regardless of drug exposure. Because trimeric complex formation depends on binding affinities to each target, Paper III explored *in silico* the impact of FAP-binding affinity on trimeric complex formation with virtual FAP-4-1BBL molecules. The impact of 4-1BB binding affinity was not considered in the work because it was assumed that the relationship between the number of trimeric complexes formed and effect remains as observed in Paper II. In reality, changes in 4-1BB binding affinity may have required protein conformational changes in the antibody design leading to different pharmacology after trimeric complex formation.

Our findings suggest that a 10-fold increase in FAP-binding affinity would increase the percentage of patients expected to achieve 90% of the maximum pharmacological effect from 6% to 40% in the colon cancer indication. However, it is not demonstrated that 90% of the maximum pharmacological effect is the target threshold to achieve clinical benefit. Furthermore, these simulations were conducted assuming that drug exposure leading to maximum trimeric complex formation can be achieved and maintained for each molecule. In practice, it cannot be excluded that a higher FAP-binding affinity leads to stronger TMDD and a faster PK profile. Furthermore, in optimizing for increased trimeric complex formation, our work assumes no safety liabilities with increased trimeric complex formation. Although this might be true for molecules targeting FAP (whose expression is confined to tumor stroma and tumor-draining lymph nodes), other tumor targets expressed in healthy tissues may not allow to increase binding affinity without compromising safety. In these cases, however, instead of solely optimizing trimeric complex formation during *in silico* binding affinity selection, the difference in trimeric complex formation between tumor and healthy tissues could be considered as a combined surrogate marker of safety and efficacy.

In conclusion, our results highlight the potential of combining knowledge on clinical target expression, preliminary pharmacology results from a candidate molecule as well as quantitative modeling and simulation as a tool to guide the design of bispecific costimulators. Indeed, preclinical experiments have already been performed with molecules that vary both in the tumor target and in the T-cell target binding affinity (105). With our approach, we believe that knowledge of clinical target expression can also be incorporated into the decision-making process, providing a prediction of the binding affinities expected to lead to the desired pharmacological profile. Then, these molecules can be engineered without the need of iterating experimentally across the whole space of binding affinities.

Quantifying the impact of ADAs on drug exposure with biologics

Regardless of how promising a drug candidate is in preclinical development, or how well-designed the clinical strategy is, success with cancer immunotherapies necessarily involves understanding the dose-exposure-response relationship in the clinic.

Many of the cancer immunotherapies under development represent different classes of mAbs, which differ from naturally occurring immunoglobulins both in amino acid sequence and three-dimensional structure. As a result, many of these molecules induce ADA formation, which can in turn trigger drug exposure loss. In Paper IV, a semimechanistic model accounting for ADA formation over time, ADA binding to cibisatamab in the central compartment, and increased cibisatamab elimination as a result of ADA binding, was developed. The model successfully described a variety of PK profiles simultaneously, both in presence and absence of ADA formation.

The developed model was then used to explore potential relationships between patient covariates and dosing regimen with ADA-driven loss of exposure. Although no relationship was found, similar analysis can be performed with other biologics to elucidate on a case-by-case basis whether these variables may impact ADA formation (thus suggesting potential mitigation strategies). Indeed, the only factor that was found to be related to decreased ADA formation and decreased ADA-driven exposure loss was pretreatment with the CD20-directed antibody obinutuzumab, which has already been shown to be a feasible strategy to reduce ADA formation (106).

The developed model can describe PK of patients displaying different patterns of loss of exposure (*e.g.* reduced Ctrough exposure, transient ADA formation followed by exposure recovery later on, or total loss of exposure, with no PK sample above the LLOQ during the treatment cycle). As a result, the model can serve as PK input for further PK/PD model development without

the need to exclude patients with ADA exposure loss. This is of particular interest when developing TCBs, as it allows differentiating tumor regrowth due to emergence of resistance mechanisms from tumor regrowth due to ADA-driven loss of TCB exposure. However, because the model could not relate dose and dosing schedule to ADA formation, it does not allow simulating the expected exposure under different dosing strategies.

Conclusions

This thesis developed modeling and simulation approaches to guide the development of cancer immunotherapy combinations by optimizing molecule design, preclinical experiment design, and translation of preclinical knowledge into clinical insights.

The findings suggest that TCBs in solid tumors may elicit their full potential only in combination with other cancer immunotherapies. Therefore, if preclinical modeling suggests that the TCB may not work as a single agent and may be more promising in combination, the clinical testing of such combination should not be dependent on the efficacy results of the monotherapy study. This was demonstrated with the case-example of TYRP1-TCB, a TCB studied in advanced melanoma patients, in combination with an anti-PD-L1 CPI.

Bispecific costimulator antibodies may be an ideal combination partner for TCBs, as they can provide additional T-cell activation and prevent T-cell exhaustion. However, preclinical data combined with mathematical modeling suggests that the exposure-effect relationship with these molecules follows a bell-shaped curve, which poses challenges for dose selection. The developed workflow can integrate data from standard *in vitro* experiments to suggest the range of exposures with bispecific costimulators that maximizes the effect, and what doses to explore in the clinic. Additionally, the model allowed deconvoluting the role that bispecific antibody exposure and target expression play in tumor cell killing, further clarifying the drivers of effect with bispecific costimulators. Using the case-example of the costimulator FAP-4-1BBL in combination with the TCB cibisatamab, a range of doses expected to maximize effect was proposed, and the threshold of FAP expression to achieve 90% of the maximum effect was established.

In a further step, *in silico* studies demonstrated that a 10-fold increase in FAP-binding affinity is expected to increase the percentage of patients achieving 90% of the maximum effect with FAP-targeted bispecific costimulators across several solid tumor indications. It was illustrated how a model-informed drug development (MIDD) approach can add value at the discovery stages using the case-example of FAP-4-1BBL. The findings suggest that a ten-fold increase in FAP-binding affinity may markedly increase the percentage of patients who can derive clinical benefit from the molecule, compared to the current FAP-4-1BBL molecule.

Lastly, despite the promising preclinical pharmacology of these bispecific molecules, they may elicit immunogenicity when administered to humans, which results in decreased drug exposure. The developed population PK model can be used to semimechanistically describe the formation of ADAs and their impact on drug exposure, which in turn allows not only the inclusion of all patients in exposure-response analyses, but also to investigate whether patient covariates or the treatment schedule are related to immunogenicity. Using cibisatamab as a case-example, no effect of patient covariates or dosing schedule was observed on ADA formation or ADA impact on exposure loss.

Future perspectives

Although this thesis has provided a toolkit of methods and workflows to optimize cancer immunotherapy combinations using preclinical data and mathematical modeling and simulation, it also opens new horizons for exploration. In particular, the key topic of translatability of predictions based on models developed with preclinical data is still pending.

Specifically, whether the observed TGI profile in mice treated with TCBs as single agent or in combination with CPIs translates to the clinic needs to be validated using clinical data. A first step to do so (the characterization of the PK of the TCB even in the presence of ADAs, which frequently arise during treatment with TCBs) has already been tackled, but no TGI model using clinical data of patients with solid tumors treated with a TCB has been developed to date. Developing such model could inform not only whether the shape of the TGI curve versus time is like that observed in mouse (tumor shrinkage followed by fast tumor regrowth), but also whether increased doses or combination with CPIs delay time to tumor regrowth to a similar extent as observed in mouse. It can be envisioned that developing such a model with clinical data will have to deal with less granularity in the tumor measurements, patient dropout as soon as progression is detected, and a more variable environment than that of preclinical experiments. An intermediate step to evaluate the feasibility of such analysis could simulate clinical tumor growth inhibition data based on the TGI model from mouse translated to human (with tumor scans following the RECIST recommendations for response assessment, as would be the case in a clinical trial). Next, the original tumor growth inhibition model developed in mouse could be re-estimated using this data, to gain insights on whether the clinical data supports such a model development, or whether simpler model structures may be required simply because of sparser data.

The exposure-response with bispecific costimulators has been proposed to follow a bell-shaped curve, but solid clinical evidence of this phenomenon is lacking. In this thesis, the impact of target expression (frequently an uncontrolled variable in early-stage clinical trials) on pharmacology with bispecific antibodies has been evaluated. A similar model-based analysis (based on trimeric complex formation, rather than exposure) could be pursued using clinical data with bispecific costimulators to inform on whether the bell-shaped dose-response that is expected from preclinical data and mathematical modeling is indeed observed in the clinic. The key point of interest here would be

whether the exposure leading to maximum trimeric complex formation (and hence, effect) remains unchanged versus *in vitro* or preclinical *in vivo* data. Although this would greatly simplify human efficacious dose estimation based on preclinical data, such validation would require a more quantitative understanding of the target expression. As demonstrated in this work, IHC-based measurements of target expression in the tumor may not provide sufficient information to establish the trimeric complex-response relationship. An analysis using different surrogates for target expression in the clinic (*e.g.* RNA-seq, soluble target in plasma, PET uptake) could also provide insights on whether these alternatives can better capture the differences in response that may be expected due to differences in target expression.

Using the developed modeling and simulation workflows, a proposal to select binding affinities for tumor-targeted bispecific costimulators has been made, although these virtual molecules have not been tested experimentally. To validate this workflow, the virtual molecules of highest interest could be synthesized, and the standard battery of *in vitro* experiments could be run. Of particular interest in this analysis would be to inspect whether the bell-shaped exposure-response curve shifts its maximum (as predicted) towards lower exposures, with greater amplitude in the curve, and whether the relationship between trimeric complex and pharmacology remains constant (as assumed in the work).

Furthermore, this optimization workflow has been developed with efficacy in mind; a next step could include and explore the effects of binding affinity on safety. To do so, a prerequisite would be to establish the quantitative relationship between trimeric complex formation and a safety biomarker *in vitro* (such as cytokine release). Next, target expressions both on-tumor and off-tumor can be retrieved from the literature. With this, the expected cytokine release (acting as a safety biomarker) and tumor cell killing (acting as an efficacy surrogate) can be anticipated at different binding affinities, offering insights into the optimal binding affinity that maximizes not solely efficacy, but also safety. On a case-by-case basis, safety or efficacy can be optimized for (depending, for example, on the expected extent of off-tumor target expression).

Acknowledgements

The work presented in this thesis was conducted at the Department of Pharmacy of Uppsala University (Sweden), in collaboration with F. Hoffman-La Roche Ltd. (Basel, Switzerland). I will be forever grateful to Roche and to the Predictive Modeling and Data Analytics chapter within Pharma Research and Early Development for giving me the opportunity of doing an industry PhD for 4 years (plus 8 months as an intern prior to the PhD start).

The number of people that I must thank is immense, and I fear I will forget many of them. I never let perfect be the enemy of good, so I will still try to draft some words of acknowledgment to as many people as possible, but I apologize in advance for those who may not appear and most certainly deserve it.

No PhD at all would have been possible without the relentless support of my industry supervisor and mentor, Dr. Nicolas Frances. We first started working together with a 6-month internship in February 2020, and four years and eight months later, we submitted the last manuscript that constitutes this thesis. During that time, I have learned more than I ever thought, and I was blessed with more confidence than perhaps I ever deserved. This certainly prepared me for what I hope will be a fruitful career in drug development. *Merci beaucoup*, Nicolas. This is a small world and I hope we will cross paths again.

None of this work would have been possible without the help of (and bi-weekly meetings with) my academic supervisors, Lena Friberg and Siv Jönsson. Thank you for always being able to find the time to discuss, for being able to navigate all the back-and-forth communications between industry and academia, for your input on all the projects, for your guidance on all the manuscripts, for helping me out with my not-so-good English writing, for your patience with me. I hope we can stay in touch in the relatively small (but fast-growing) world of pharmacometrics. There could have been no better academic partner than Uppsala University, and I could have not dreamt of better mentors than you.

I thank all the Uppsala colleagues who have helped me out every time I needed it, from whom I have learned so many things, and whom I have, most certainly, annoyed at some point during the last four years. Thank you for everything.

I need to extend my thanks to many of my Roche colleagues, but if I had to write all the names, the list would be longer than the thesis. I thank all the members of the Translational Modeling & Simulation capability, which is full

of awesome scientists and even better human beings. I thank all my other PMDA colleagues for creating a group with a great atmosphere where I always felt welcomed. I thank the other PhD students at Roche for building a community where I always felt supported. I thank specifically my fellow modeling PhD students: Agustos, for the nice drinks letting off some steam on Friday evenings and your positivity, Yann, for the very interesting scientific discussions and your effort setting up the PhD student community, Apolline, for the coffees every morning, the moral support, and the learnings together.

I thank my friends in Spain, for always making time for me even if I only visit twice per year and on short notice. I thank my friends in Basel: I arrived there for my first international experience, originally for six months, of which five were of COVID pandemic, and in just one summer together you made me feel at home.

I thank my family for the continuous support during these years, for your interest in what I do (even if I never managed to explain it as easily as I should). My only regret with this PhD is choosing a professional path that may keep me far from you for a very long time. I know you understand it, *pero eso no lo hace más fácil*.

I want to thank my partner for her support during my PhD, for her input with our scientific discussions, for always cheering me up, for always helping me out. Because the best thing about getting into Modeling and Simulation was meeting you at PAGE. That made everything worth it.

References

1. Vaddepally RK, Kharel P, Pandey R, Garje R, Chandra AB. Review of Indications of FDA-Approved Immune Checkpoint Inhibitors per NCCN Guidelines with the Level of Evidence. Cancers. 2020 Mar;12(3):738.
2. Haslam A, Prasad V. Estimation of the Percentage of US Patients With Cancer Who Are Eligible for and Respond to Checkpoint Inhibitor Immunotherapy Drugs. JAMA Netw Open. 2019 May 3;2(5):e192535.
3. Yap TA, Parkes EE, Peng W, Moyers JT, Curran MA, Tawbi HA. Development of Immunotherapy Combination Strategies in Cancer. Cancer Discov. 2021 Jun 1;11(6):1368–97.
4. Chelliah V, Lazarou G, Bhatnagar S, Gibbs JP, Nijsen M, Ray A, et al. Quantitative Systems Pharmacology Approaches for Immuno-Oncology: Adding Virtual Patients to the Development Paradigm. Clin Pharmacol Ther. 2021;109(3):605–18.
5. Sanchez J, Claus C, McIntyre C, Tanos T, Boehnke A, Friberg LE, et al. Combining mathematical modeling, in vitro data and clinical target expression to support bispecific antibody binding affinity selection: a case example with FAP-4-1BBL. Front Pharmacol [Internet]. 2024 Oct 9 [cited 2024 Nov 17];15. Available from: https://www.frontiersin.org/journals/pharmacology/articles/10.3389/fphar.2024.1472662/full
6. Waldman AD, Fritz JM, Lenardo MJ. A guide to cancer immunotherapy: from T cell basic science to clinical practice. Nat Rev Immunol. 2020 Nov;20(11):651–68.
7. Strohl WR, Naso M. Bispecific T-Cell Redirection versus Chimeric Antigen Receptor (CAR)-T Cells as Approaches to Kill Cancer Cells. Antibodies. 2019 Sep;8(3):41.
8. Blache U, Popp G, Dünkel A, Koehl U, Fricke S. Potential solutions for manufacture of CAR T cells in cancer immunotherapy. Nat Commun. 2022 Sep 5;13(1):5225.
9. San-Miguel J, Dhakal B, Yong K, Spencer A, Anguille S, Mateos MV, et al. Cilta-cel or Standard Care in Lenalidomide-Refractory Multiple Myeloma. N Engl J Med. 2023 Jul 26;389(4):335–47.
10. Locke FL, Miklos DB, Jacobson CA, Perales MA, Kersten MJ, Oluwole OO, et al. Axicabtagene Ciloleucel as Second-Line Therapy for Large B-Cell Lymphoma. N Engl J Med. 2022 Feb 16;386(7):640–54.
11. Mohyuddin GR, Atieh T, Ahmed N, Sborov D, McClune B, Abdallah AO, et al. Intention to treat versus modified intention-to-treat analysis in B-cell maturation antigen and CD19 chimeric antigen receptor trials: A systematic review and meta-analysis. Eur J Cancer. 2021 Oct 1;156:164–74.
12. Abou-el-Enein M, Elsallab M, Feldman SA, Fesnak AD, Heslop HE, Marks P, et al. Scalable Manufacturing of CAR T Cells for Cancer Immunotherapy. Blood Cancer Discov. 2021 Aug 3;2(5):408.

13. Albelda SM. CAR T cell therapy for patients with solid tumours: key lessons to learn and unlearn. Nat Rev Clin Oncol. 2024 Jan;21(1):47–66.
14. Trabolsi A, Arumov A, Schatz JH. Bispecific antibodies and CAR-T cells: dueling immunotherapies for large B-cell lymphomas. Blood Cancer J. 2024 Feb 8;14(1):1–10.
15. Liu J, Zhu J. Progresses of T-cell-engaging bispecific antibodies in treatment of solid tumors. Int Immunopharmacol. 2024 Sep 10;138:112609.
16. Seager RJ, Hajal C, Spill F, Kamm RD, Zaman MH. Dynamic interplay between tumour, stroma and immune system can drive or prevent tumour progression. Converg Sci Phys Oncol. 2017 Jul 28;3:034002.
17. Gerard CL, Delyon J, Wicky A, Homicsko K, Cuendet MA, Michielin O. Turning tumors from cold to inflamed to improve immunotherapy response. Cancer Treat Rev. 2021 Dec 1;101:102227.
18. Leivonen SK, Pollari M, Brück O, Pellinen T, Autio M, Karjalainen-Lindsberg ML, et al. T-cell inflamed tumor microenvironment predicts favorable prognosis in primary testicular lymphoma. Haematologica. 2018 Sep 20;104(2):338.
19. Bruni S, Mercogliano MF, Mauro FL, Cordo Russo RI, Schillaci R. Cancer immune exclusion: breaking the barricade for a successful immunotherapy. Front Oncol [Internet]. 2023 May 22 [cited 2024 Nov 17];13. Available from: https://www.frontiersin.org/journals/oncology/articles/10.3389/fonc.2023.1135456/full
20. Coto-Llerena M, Ercan C, Kancherla V, Taha-Mehlitz S, Eppenberger-Castori S, Soysal SD, et al. High Expression of FAP in Colorectal Cancer Is Associated With Angiogenesis and Immunoregulation Processes. Front Oncol. 2020 Jul 8;10:979.
21. Privé BM, Boussihmad MA, Timmermans B, van Gemert WA, Peters SMB, Derks YHW, et al. Fibroblast activation protein-targeted radionuclide therapy: background, opportunities, and challenges of first (pre)clinical studies. Eur J Nucl Med Mol Imaging. 2023 Jun 1;50(7):1906–18.
22. Claus C, Ferrara C, Xu W, Sam J, Lang S, Uhlenbrock F, et al. Tumor-targeted 4-1BB agonists for combination with T cell bispecific antibodies as off-the-shelf therapy. Sci Transl Med. 2019 Jun 12;11(496):eaav5989.
23. Marrack P, Scott-Browne J, MacLeod MKL. Terminating the Immune Response. Immunol Rev. 2010 Jul;236:5.
24. He X, Xu C. Immune checkpoint signaling and cancer immunotherapy. Cell Res. 2020 Aug;30(8):660–9.
25. Chen DS, Mellman I. Oncology Meets Immunology: The Cancer-Immunity Cycle. Immunity. 2013 Jul 25;39(1):1–10.
26. Salmaninejad A, Valilou SF, Shabgah AG, Aslani S, Alimardani M, Pasdar A, et al. PD-1/PD-L1 pathway: Basic biology and role in cancer immunotherapy. J Cell Physiol. 2019 Aug;234(10):16824–37.
27. Lin X, Kang K, Chen P, Zeng Z, Li G, Xiong W, et al. Regulatory mechanisms of PD-1/PD-L1 in cancers. Mol Cancer. 2024 May 18;23(1):108.
28. Cameron F, Whiteside G, Perry C. Ipilimumab: first global approval. Drugs. 2011 May 28;71(8):1093–104.
29. Keam SJ. Tremelimumab: First Approval. Drugs. 2023 Jan;83(1):93–102.
30. Paik J. Nivolumab Plus Relatlimab: First Approval. Drugs. 2022 Jun;82(8):925–31.
31. Dziadziuszko R, Ahn MJ, Kelly K, Popat S, Wakelee HA, Baird AM, et al. SKYSCRAPER-03: A Phase III, Open-Label, Randomized Study of Atezolizumab Plus Tiragolumab Compared With Durvalumab in Patients With Locally Advanced, Unresectable, Stage III NSCLC Who Have Not Progressed After Platinum-Based Concurrent Chemoradiation. Int J Radiat Oncol Biol Phys. 2021 Nov 1;111(3):e420–1.

32. Cai L, Li Y, Tan J, Xu L, Li Y. Targeting LAG-3, TIM-3, and TIGIT for cancer immunotherapy. J Hematol OncolJ Hematol Oncol. 2023 Sep 5;16(1):101.
33. Eng C, Kim TW, Bendell J, Argilés G, Tebbutt NC, Bartolomeo MD, et al. Atezolizumab with or without cobimetinib versus regorafenib in previously treated metastatic colorectal cancer (IMblaze370): a multicentre, open-label, phase 3, randomised, controlled trial. Lancet Oncol. 2019 Jun 1;20(6):849–61.
34. Sahin IH, Ciombor KK, Diaz LA, Yu J, Kim R. Immunotherapy for Microsatellite Stable Colorectal Cancers: Challenges and Novel Therapeutic Avenues. Am Soc Clin Oncol Educ Book. 2022 Jun 3;(42):242–53.
35. Reck M, Rodríguez-Abreu D, Robinson AG, Hui R, Csőszi T, Fülöp A, et al. Pembrolizumab versus Chemotherapy for PD-L1–Positive Non–Small-Cell Lung Cancer. N Engl J Med. 2016 Nov 10;375(19):1823–33.
36. Tawbi HA, Schadendorf D, Lipson EJ, Ascierto PA, Matamala L, Gutiérrez EC, et al. Relatlimab and Nivolumab versus Nivolumab in Untreated Advanced Melanoma. N Engl J Med. 2022 Jan 5;386(1):24–34.
37. Larkin J, Chiarion-Sileni V, Gonzalez R, Grob JJ, Rutkowski P, Lao CD, et al. Five-Year Survival with Combined Nivolumab and Ipilimumab in Advanced Melanoma. N Engl J Med. 2019 Oct 17;381(16):1535–46.
38. Abou-Alfa GK, Lau G, Kudo M, Chan SL, Kelley RK, Furuse J, et al. Tremelimumab plus Durvalumab in Unresectable Hepatocellular Carcinoma. NEJM Evid. 2022 Jul 26;1(8):EVIDoa2100070.
39. Zhou S, Liu M, Ren F, Meng X, Yu J. The landscape of bispecific T cell engager in cancer treatment. Biomark Res. 2021 May 26;9(1):38.
40. Bacac M, Colombetti S, Herter S, Sam J, Perro M, Chen S, et al. CD20-TCB with Obinutuzumab Pretreatment as Next-Generation Treatment of Hematologic Malignancies. Clin Cancer Res Off J Am Assoc Cancer Res. 2018 Oct 1;24(19):4785–97.
41. Bacac M, Fauti T, Sam J, Colombetti S, Weinzierl T, Ouaret D, et al. A Novel Carcinoembryonic Antigen T-Cell Bispecific Antibody (CEA TCB) for the Treatment of Solid Tumors. Clin Cancer Res Off J Am Assoc Cancer Res. 2016 Jul 1;22(13):3286–97.
42. Saeed A, Park R, Pathak H, Al-Bzour AN, Dai J, Phadnis M, et al. Clinical and biomarker results from a phase II trial of combined cabozantinib and durvalumab in patients with chemotherapy-refractory colorectal cancer (CRC): CAMILLA CRC cohort. Nat Commun. 2024 Feb 20;15(1):1533.
43. Iurlaro R, Waldhauer I, Planas-Rigol E, Bonfill-Teixidor E, Arias A, Nicolini V, et al. A Novel EGFRvIII T-Cell Bispecific Antibody for the Treatment of Glioblastoma. Mol Cancer Ther. 2022 Oct 7;21(10):1499–509.
44. Segal NH, Melero I, Moreno V, Steeghs N, Marabelle A, Rohrberg K, et al. CEA-CD3 bispecific antibody cibisatamab with or without atezolizumab in patients with CEA-positive solid tumours: results of two multi-institutional Phase 1 trials. Nat Commun. 2024 May 15;15(1):4091.
45. Kang C. Mosunetuzumab: First Approval. Drugs. 2022 Jul;82(11):1229–34.
46. Shirley M. Glofitamab: First Approval. Drugs. 2023 Jul;83(10):935–41.
47. Frampton JE. Epcoritamab: First Approval. Drugs. 2023 Sep;83(14):1331–40.
48. Dhillon S. Elranatamab: First Approval. Drugs. 2023 Nov;83(17):1621–7.
49. Keam SJ. Talquetamab: First Approval. Drugs. 2023 Oct;83(15):1439–45.
50. Kang C. Teclistamab: First Approval. Drugs. 2022 Nov;82(16):1613–9.
51. Carvajal RD, Butler MO, Shoushtari AN, Hassel JC, Ikeguchi A, Hernandez-Aya L, et al. Clinical and molecular response to tebentafusp in previously treated patients with metastatic uveal melanoma: a phase 2 trial. Nat Med. 2022 Nov;28(11):2364–73.

52. Meermeier EW, Welsh SJ, Sharik ME, Du MT, Garbitt VM, Riggs DL, et al. Tumor burden limits bispecific antibody efficacy through T cell exhaustion averted by concurrent cytotoxic therapy. Blood Cancer Discov. 2021 Jul;2(4):354–69.
53. Junttila TT, Li J, Johnston J, Hristopoulos M, Clark R, Ellerman D, et al. Antitumor Efficacy of a Bispecific Antibody That Targets HER2 and Activates T Cells. Cancer Res. 2014 Sep 30;74(19):5561–71.
54. Gonzalez-Exposito R, Semiannikova M, Griffiths B, Khan K, Barber LJ, Woolston A, et al. CEA expression heterogeneity and plasticity confer resistance to the CEA-targeting bispecific immunotherapy antibody cibisatamab (CEA-TCB) in patient-derived colorectal cancer organoids. J Immunother Cancer. 2019 Apr 15;7(1):101.
55. Dorff T, Horvath LG, Autio K, Bernard-Tessier A, Rettig MB, Machiels JP, et al. A Phase I Study of Acapatamab, a Half-life Extended, PSMA-Targeting Bispecific T-cell Engager for Metastatic Castration-Resistant Prostate Cancer. Clin Cancer Res Off J Am Assoc Cancer Res. 2024 Apr 15;30(8):1488–500.
56. Spreafico A, Couselo EM, Irmisch A, Bessa J, Au-Yeung G, Bechter O, et al. Phase 1, first-in-human study of TYRP1-TCB (RO7293583), a novel TYRP1-targeting CD3 T-cell engager, in metastatic melanoma: active drug monitoring to assess the impact of immune response on drug exposure. Front Oncol [Internet]. 2024 Mar 21 [cited 2024 Nov 18];14. Available from: https://www.frontiersin.org/journals/oncology/articles/10.3389/fonc.2024.1346502/full
57. Sam J, Colombetti S, Fauti T, Roller A, Biehl M, Fahrni L, et al. Combination of T-Cell Bispecific Antibodies With PD-L1 Checkpoint Inhibition Elicits Superior Anti-Tumor Activity. Front Oncol. 2020 Nov 30;10:575737.
58. Nicolini VG, Waldhauer I, Freimoser-Grundschober A, Richard M, Fahrni L, Bommer E, et al. Abstract LB-389: Combination of TYRP1-TCB, a novel T cell bispecific antibody for the treatment of melanoma, with immunomodulatory agents. Cancer Res. 2020 Aug 15;80(16_Supplement):LB-389.
59. Stein MN, Zhang J, Kelly WK, Wise DR, Tsao K, Carneiro BA, et al. Preliminary results from a phase 1/2 study of co-stimulatory bispecific PSMAxCD28 antibody REGN5678 in patients (pts) with metastatic castration-resistant prostate cancer (mCRPC). J Clin Oncol. 2023 Feb 20;41(6_suppl):154–154.
60. Mariuzza RA, Agnihotri P, Orban J. The structural basis of T-cell receptor (TCR) activation: An enduring enigma. J Biol Chem. 2019 Dec 17;295(4):914.
61. Fisher TS, Kamperschroer C, Oliphant T, Love VA, Lira PD, Doyonnas R, et al. Targeting of 4-1BB by monoclonal antibody PF-05082566 enhances T-cell function and promotes anti-tumor activity. Cancer Immunol Immunother CII. 2012 Oct;61(10):1721–33.
62. Palazón A, Teijeira A, Martínez-Forero I, Hervás-Stubbs S, Roncal C, Peñuelas I, et al. Agonist anti-CD137 mAb act on tumor endothelial cells to enhance recruitment of activated T lymphocytes. Cancer Res. 2011 Feb 1;71(3):801–11.
63. Esensten JH, Helou YA, Chopra G, Weiss A, Bluestone JA. CD28 costimulation: from mechanism to therapy. Immunity. 2016 May 17;44(5):973.
64. Khushalani NI, Ott PA, Ferris RL, Cascone T, Schadendorf D, Le DT, et al. Final results of urelumab, an anti-CD137 agonist monoclonal antibody, in combination with cetuximab or nivolumab in patients with advanced solid tumors. J Immunother Cancer. 2024 Mar 1;12(3):e007364.
65. Attarwala H. TGN1412: From Discovery to Disaster. J Young Pharm. 2010 Jul 1;2(3):332–6.

66. Shen A, Liu W, Wang H, Zeng X, Wang M, Zhang D, et al. A novel 4-1BB/HER2 bispecific antibody shows potent antitumor activities by increasing and activating tumor-infiltrating T cells. Am J Cancer Res. 2023 Jul 15;13(7):3246.
67. Liang J, Su C, Peng H, Hao F, Liu T, Ning J, et al. Abstract 2381: The bispecific antibody KA-3001, targeting PSMA and CD28, specifically enhances T cell activation within prostate tumors. Cancer Res. 2024 Mar 22;84(6_Supplement):2381.
68. Eisenhauer EA, Therasse P, Bogaerts J, Schwartz LH, Sargent D, Ford R, et al. New response evaluation criteria in solid tumours: Revised RECIST guideline (version 1.1). Eur J Cancer. 2009 Jan;45(2):228–47.
69. Betts A, Keunecke A, van Steeg TJ, van der Graaf PH, Avery LB, Jones H, et al. Linear pharmacokinetic parameters for monoclonal antibodies are similar within a species and across different pharmacological targets: A comparison between human, cynomolgus monkey and hFcRn Tg32 transgenic mouse using a population-modeling approach. mAbs. 2018 Jul;10(5):751–64.
70. Sánchez J, Claus C, Albrecht R, Gaillard BC, Marinho J, McIntyre C, et al. A model-based approach leveraging in vitro data to support dose selection from the outset: A framework for bispecific antibodies in immuno-oncology. CPT Pharmacomet Syst Pharmacol. 2023;12(11):1804–18.
71. Liu Y, Wu W, Cai C, Zhang H, Shen H, Han Y. Patient-derived xenograft models in cancer therapy: technologies and applications. Signal Transduct Target Ther. 2023 Apr 12;8(1):1–24.
72. Cogels MM, Rouas R, Ghanem GE, Martinive P, Awada A, Gestel DV, et al. Humanized Mice as a Valuable Pre-Clinical Model for Cancer Immunotherapy Research. Front Oncol. 2021 Nov 18;11:784947.
73. Stripecke R, Münz C, Schuringa JJ, Bissig KD, Soper B, Meeham T, et al. Innovations, challenges, and minimal information for standardization of humanized mice. EMBO Mol Med. 2020 Jun 24;12(7):e8662.
74. Toloi D de A, Jardim DLF, Hoff PMG, Riechelmann RSP. Phase I trials of antitumour agents: fundamental concepts. ecancermedicalscience. 2015 Jan 19;9:501.
75. Takimoto CH. Maximum tolerated dose: clinical endpoint for a bygone era? Target Oncol. 2009 Apr;4(2):143–7.
76. Shah M, Rahman A, Theoret MR, Pazdur R. The Drug-Dosing Conundrum in Oncology — When Less Is More. N Engl J Med. 2021 Oct 13;385(16):1445–7.
77. Jawa V, Terry F, Gokemeijer J, Mitra-Kaushik S, Roberts BJ, Tourdot S, et al. T-Cell Dependent Immunogenicity of Protein Therapeutics Pre-clinical Assessment and Mitigation–Updated Consensus and Review 2020. Front Immunol [Internet]. 2020 Jun 30 [cited 2024 Nov 18];11. Available from: https://www.frontiersin.org/journals/immunology/articles/10.3389/fimmu.2020.01301/full
78. Ciano-Petersen NL, Aliaga-Gaspar P, Hurtado-Guerrero I, Reyes V, Rodriguez-Bada JL, Rodriguez-Traver E, et al. Natalizumab-immunogenicity evaluation in patients with infusion related events or disease exacerbations. Front Immunol. 2023;14:1242508.
79. Moots RJ, Xavier RM, Mok CC, Rahman MU, Tsai WC, Al-Maini MH, et al. The impact of anti-drug antibodies on drug concentrations and clinical outcomes in rheumatoid arthritis patients treated with adalimumab, etanercept, or infliximab: Results from a multinational, real-world clinical practice, non-interventional study. PloS One. 2017;12(4):e0175207.

80. Hellmann MD, Bivi N, Calderon B, Shimizu T, Delafontaine B, Liu ZT, et al. Safety and Immunogenicity of LY3415244, a Bispecific Antibody Against TIM-3 and PD-L1, in Patients With Advanced Solid Tumors. Clin Cancer Res. 2021 May 15;27(10):2773–81.
81. Ribba B, Holford N, Magni P, Trocóniz I, Gueorguieva I, Girard P, et al. A Review of Mixed-Effects Models of Tumor Growth and Effects of Anticancer Drug Treatment Used in Population Analysis. CPT Pharmacomet Syst Pharmacol. 2014;3(5):113.
82. Simeoni M, Magni P, Cammia C, De Nicolao G, Croci V, Pesenti E, et al. Predictive Pharmacokinetic-Pharmacodynamic Modeling of Tumor Growth Kinetics in Xenograft Models after Administration of Anticancer Agents. Cancer Res. 2004 Feb 10;64(3):1094–101.
83. Jones RDO, Grondine M, Borodovsky A, San Martin M, DuPont M, D'Cruz C, et al. A pharmacokinetic–pharmacodynamic model for the MET tyrosine kinase inhibitor, savolitinib, to explore target inhibition requirements for anti-tumour activity. Br J Pharmacol. 2021;178(3):600–13.
84. Chatterjee M, Elassaiss-Schaap J, Lindauer A, Turner D, Sostelly A, Freshwater T, et al. Population Pharmacokinetic/Pharmacodynamic Modeling of Tumor Size Dynamics in Pembrolizumab-Treated Advanced Melanoma. CPT Pharmacomet Syst Pharmacol. 2017;6(1):29–39.
85. Ribba B, Kaloshi G, Peyre M, Ricard D, Calvez V, Tod M, et al. A Tumor Growth Inhibition Model for Low-Grade Glioma Treated with Chemotherapy or Radiotherapy. Clin Cancer Res. 2012 Sep 16;18(18):5071–80.
86. Betts A, van der Graaf PH. Mechanistic Quantitative Pharmacology Strategies for the Early Clinical Development of Bispecific Antibodies in Oncology. Clin Pharmacol Ther. 2020 Sep;108(3):528–41.
87. Betts A, Haddish-Berhane N, Shah DK, van der Graaf PH, Barletta F, King L, et al. A Translational Quantitative Systems Pharmacology Model for CD3 Bispecific Molecules: Application to Quantify T Cell-Mediated Tumor Cell Killing by P-Cadherin LP DART®. AAPS J. 2019 May 22;21(4):66.
88. Flowers D, Bassen D, Kapitanov GI, Marcantonio D, Burke JM, Apgar JF, et al. A next generation mathematical model for the in vitro to clinical translation of T-cell engagers. J Pharmacokinet Pharmacodyn. 2023 Jun 1;50(3):215–27.
89. de Vries TJ, Trancikova D, Ruiter DJ, van Muijen GN. High expression of immunotherapy candidate proteins gp100, MART-1, tyrosinase and TRP-1 in uveal melanoma. Br J Cancer. 1998 Nov;78(9):1156–61.
90. de Vries TJ, Fourkour A, Wobbes T, Verkroost G, Ruiter DJ, van Muijen GN. Heterogeneous expression of immunotherapy candidate proteins gp100, MART-1, and tyrosinase in human melanoma cell lines and in human melanocytic lesions. Cancer Res. 1997 Aug 1;57(15):3223–9.
91. Beal SL. Ways to fit a PK model with some data below the quantification limit. J Pharmacokinet Pharmacodyn. 2001 Oct;28(5):481–504.
92. Chen X, Hickling T, Kraynov E, Kuang B, Parng C, Vicini P. A Mathematical Model of the Effect of Immunogenicity on Therapeutic Protein Pharmacokinetics. AAPS J. 2013 Aug 30;15(4):1141–54.
93. Lavielle M, Mbogning C. An improved SAEM algorithm for maximum likelihood estimation in mixtures of non linear mixed effects models. Stat Comput. 2014 Sep 1;24(5):693–707.
94. Lindauer A, Valiathan C, Mehta K, Sriram V, de Greef R, Elassaiss-Schaap J, et al. Translational Pharmacokinetic/Pharmacodynamic Modeling of Tumor Growth Inhibition Supports Dose-Range Selection of the Anti–PD-1 Antibody Pembrolizumab. CPT Pharmacomet Syst Pharmacol. 2017;6(1):11–20.

95. Zboralski D, Hoehne A, Bredenbeck A, Schumann A, Nguyen M, Schneider E, et al. Preclinical evaluation of FAP-2286 for fibroblast activation protein targeted radionuclide imaging and therapy. Eur J Nucl Med Mol Imaging. 2022 Sep 1;49(11):3651–67.
96. Micallef S, Morcos PN, McIntyre C, Frey N, Buchheit V, Canadi J, et al. Using population pharmacokinetics to capture the binding of a novel bispecific fibroblast activation protein (FAP) to its 4-1BB ligand (4-1BBL) and support phase 2 dose selection in oncology patients. ACoP11. Virtual. In 2020.
97. Rohaan MW, Borch TH, Berg JH van den, Met Ö, Kessels R, Foppen MHG, et al. Tumor-Infiltrating Lymphocyte Therapy or Ipilimumab in Advanced Melanoma. N Engl J Med. 2022 Dec 7;387(23):2113–25.
98. Miles D, Gligorov J, André F, Cameron D, Schneeweiss A, Barrios C, et al. Primary results from IMpassion131, a double-blind, placebo-controlled, randomised phase III trial of first-line paclitaxel with or without atezolizumab for unresectable locally advanced/metastatic triple-negative breast cancer. Ann Oncol. 2021 Aug 1;32(8):994–1004.
99. Kelley RK, Ueno M, Yoo C, Finn RS, Furuse J, Ren Z, et al. Pembrolizumab in combination with gemcitabine and cisplatin compared with gemcitabine and cisplatin alone for patients with advanced biliary tract cancer (KEYNOTE-966): a randomised, double-blind, placebo-controlled, phase 3 trial. The Lancet. 2023 Jun 3;401(10391):1853–65.
100. Gyawali B, Prasad V. Drugs that lack single-agent activity: are they worth pursuing in combination? Nat Rev Clin Oncol. 2017 Apr;14(4):193–4.
101. Muik A, Garralda E, Altintas I, Gieseke F, Geva R, Ben-Ami E, et al. Preclinical Characterization and Phase I Trial Results of a Bispecific Antibody Targeting PD-L1 and 4-1BB (GEN1046) in Patients with Advanced Refractory Solid Tumors. Cancer Discov. 2022 May 2;12(5):1248–65.
102. Van De Vyver AJ, Weinzierl T, Eigenmann MJ, Frances N, Herter S, Buser RB, et al. Predicting Tumor Killing and T-Cell Activation by T-Cell Bispecific Antibodies as a Function of Target Expression: Combining In Vitro Experiments with Systems Modeling. Mol Cancer Ther. 2021 Feb 5;20(2):357–66.
103. Douglass EFJr, Miller CJ, Sparer G, Shapiro H, Spiegel DA. A Comprehensive Mathematical Model for Three-Body Binding Equilibria. J Am Chem Soc. 2013 Apr 24;135(16):6092–9.
104. Ahn MJ, Cho BC, Felip E, Korantzis I, Ohashi K, Majem M, et al. Tarlatamab for Patients with Previously Treated Small-Cell Lung Cancer. N Engl J Med. 2023 Nov 29;389(22):2063–75.
105. Warmuth S, Gunde T, Snell D, Brock M, Weinert C, Simonin A, et al. Engineering of a trispecific tumor-targeted immunotherapy incorporating 4-1BB co-stimulation and PD-L1 blockade. OncoImmunology. 2021 Jan 1;10(1):2004661.
106. Peters S, Angevin E, Alonso-Gordoa T, Rohrberg K, Melero I, Mellado B, et al. Obinutuzumab Pretreatment as a Novel Approach to Mitigate Formation of Anti-Drug Antibodies Against Cergutuzumab Amunaleukin in Patients with Solid Tumors. Clin Cancer Res. 2024 Apr 15;30(8):1630–41.

Acta Universitatis Upsaliensis

Digital Comprehensive Summaries of Uppsala Dissertations from the Faculty of Pharmacy 367

Editor: The Dean of the Faculty of Pharmacy

A doctoral dissertation from the Faculty of Pharmacy, Uppsala University, is usually a summary of a number of papers. A few copies of the complete dissertation are kept at major Swedish research libraries, while the summary alone is distributed internationally through the series Digital Comprehensive Summaries of Uppsala Dissertations from the Faculty of Pharmacy. (Prior to January, 2005, the series was published under the title "Comprehensive Summaries of Uppsala Dissertations from the Faculty of Pharmacy".)

Distribution: publications.uu.se
urn:nbn:se:uu:diva-544014

ACTA UNIVERSITATIS
UPSALIENSIS
2025